AD-A061 619 ARMY ELECTRONICS RESEARCH AND DEVELOPMENT COMMAND WS--ETC F/G 4/1
MODELING THE ION CHEMISTRY OF THE D-REGION: A CASE STUDY BASED --ETC(U)
SEP 78 M G HEAPS, F E NILES, R D SEARS

UNCLASSIFIED ERADCOM/ASL-TR-0015 NL

1 OF 1
AD A061 619

END
DATE FILMED
2-79
DDC

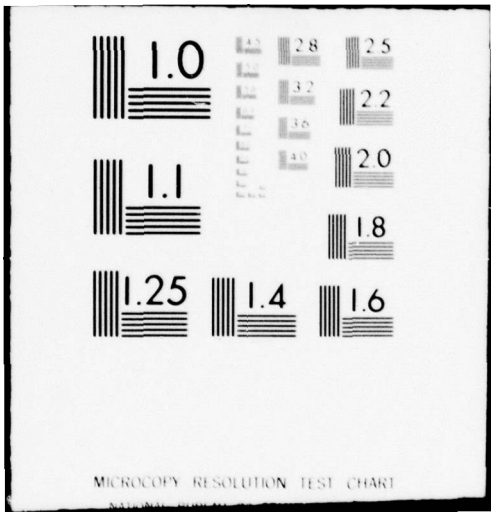
1.0
1.1
1.25
1.4
1.6
2.8
2.5
3.2
2.2
3.6
2.0
4.0
1.8
MICROCOPY RESOLUTION TEST CHART

ASL-TR-0015

LEVEL I

12

Na

AD

Reports Control Symbol
OSD - 1366

AD A061619

MODELING THE ION CHEMISTRY OF THE D-REGION: A CASE STUDY BASED UPON THE 1966 TOTAL SOLAR ECLIPSE

SEPTEMBER 1978

By

M.G. HEAPS

F.E. NILES

US ARMY ATMOSHERIC SCIENCES LABORATORY
White Sands Missile Range, New Mexico 88002

ROBERT D. SEARS

LOCKHEED PALO ALTO RESEARCH LABORATORY
Palo Alto, California

US Army Electronics Research and Development Command

Atmospheric Sciences Laboratory

White Sands Missile Range, NM 88002

NOTICES

Disclaimers

The findings in this report are not to be construed as an official Department of the Army position, unless so designated by other authorized documents.

The citation of trade names and names of manufacturers in this report is not to be construed as official Government indorsement or approval of commercial products or services referenced herein.

Disposition

Destroy this report when it is no longer needed. Do not return it to the originator.

(9) Research and development technical rept.

SECURITY CLASSIFICATION OF THIS PAGE (When Data Entered)

REPORT DOCUMENTATION PAGE

READ INSTRUCTIONS BEFORE COMPLETING FORM

(14) ERADCOM/ASL-TR-0015

1. REPORT NUMBER
2. GOVT ACCESSION NO.
3. RECIPIENT'S CATALOG NUMBER

(6) 4. TITLE (and Subtitle)

MODELING THE ION CHEMISTRY OF THE D-REGION: A CASE STUDY BASED UPON THE 1966 TOTAL SOLAR ECLIPSE.

5. TYPE OF REPORT & PERIOD COVERED

R&D Technical Report

6. PERFORMING ORG. REPORT NUMBER

(10) 7. AUTHOR(s)

M. G. Heaps,
F. E. Niles
Robert D. Sears*

8. CONTRACT OR GRANT NUMBER(s)

9. PERFORMING ORGANIZATION NAME AND ADDRESS

Atmospheric Sciences Laboratory
White Sands Missile Range, New Mexico 88002

10. PROGRAM ELEMENT, PROJECT, TASK AREA & WORK UNIT NUMBERS

(16) DA Task No. 1L162111AH71

11. CONTROLLING OFFICE NAME AND ADDRESS

US Army Electronics Research and Development Command
Adelphi, Maryland 20783

(11) 12. REPORT DATE

Sep[redacted]78

13. NUMBER OF PAGES

49

14. MONITORING AGENCY NAME & ADDRESS(if different from Controlling Office)

(12) 54p.

15. SECURITY CLASS. (of this report)

UNCLASSIFIED

15a. DECLASSIFICATION/DOWNGRADING SCHEDULE

16. DISTRIBUTION STATEMENT (of this Report)

Approved for public release; distribution unlimited.

17. DISTRIBUTION STATEMENT (of the abstract entered in Block 20, if different from Report)

18. SUPPLEMENTARY NOTES

*Lockheed Palo Alto Research Laboratory
Palo Alto, California

19. KEY WORDS (Continue on reverse side if necessary and identify by block number)

D region
Solar eclipse
Ion chemistry
Electron density
Ion density

20. ABSTRACT (Continue on reverse side if necessary and identify by block number)

The 12 November 1966 solar eclipse has been modeled by a large multi-species chemistry code and the results compared with the numerous experimental measurements which were made at that time. Good agreement between measured preeclipse values of electron density and code-predicted values is obtained when ionization by precipitating electrons from the radiation belts is included. The current gas-phase ion chemistry does not predict the rapid decrease and subsequent reconstitution of the electron density about totality in the 65 to 85 km region, nor

DD FORM 1 JAN 73 1473 EDITION OF 1 NOV 65 IS OBSOLETE

SECURITY CLASSIFICATION OF THIS PAGE (When Data Entered)

410 663

20. ABSTRACT (cont)

does it produce the large amounts of negative ions about 70 km which can be inferred from the experimental data. While basic constraints can be placed on the electron attachment processes because of the experimental data, an entirely new class of physical processes may possibly need to be included to explain this phase of D-region behavior.

Comparison with experimental data provides a means of validating the basic atmospheric modeling computer codes which are used as input for Army communication systems and in the Army nuclear weapons effect community.

PREFACE

The authors thank Mr. D. W. Hoock of Physical Sciences Laboratory, NMSU, for his assistance in compiling and running the DAIRCHEM code.

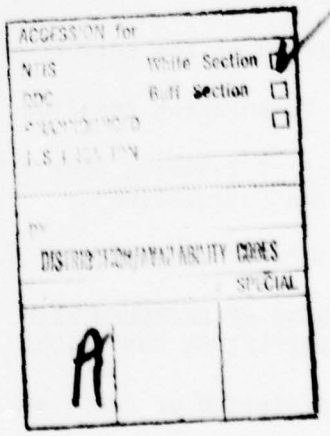

CONTENTS

INTRODUCTION

Theoretical models of the D-region have increasingly relied upon complicated computer code simulations of the chemical kinetics and photochemistry of the region. Recent progress in developing D-region models and some of the problems inherent in verification of the existing models have been outlined by Sechrist [1] and Aikin [2]. As both authors point out, progression of the complexity of D-region models from the traditional lumped parameter models (which require only single positive and negative ionic species plus electrons) to the multispecies codes places an almost impossible task upon the experimenter who seeks to verify such codes. Nevertheless, the failure of lumped parameter models to adequately describe the behavior of the D-region under even the most controlled conditions imposes the requirement for development and verification of more physically realistic kinetic chemistry models.

This report presents the results of a study which was undertaken to partially verify the D-region chemistry code known as DAIRCHEM (acronym for D-region air chemistry) which models the effects of time-varying, naturally occurring ionization sources on the chemistry of a parcel of air in the middle atmosphere. The emphasis is on the ion chemistry with sufficient neutral chemistry to make a self-consistent model.

Aikin [2] has pointed out that verification of D-region models requires data on not only the spatial and temporal distributions of the ambient ion and neutral species, but also on the ionizing source functions as well. The data base used in this study consists of an assembly of ionizing source data and models and D-region data obtained from a wide variety of experimental measurements made during the 12 November 1966 eclipse. A preliminary study which gathered these data, placed them in a common coordinate system, and defined the ionizing source functions, was conducted by Sears [3].

Comparisons with experimental data provide a means of validating the basic modeling computer codes which are used as input for Army communication systems and in the Army nuclear weapons effect community. In addition, such comparisons are a means of assessing what further experimental measurements must be made to provide data to improve already existing computer codes.

The organization of this report is as follows: "Ionospheric Measurements" describes in detail the 1966 solar eclipse experimental measurements of positive and negative ion densities versus altitude and time. "D-Region Ionizing Sources" defines the ionizing source functions appropriate to the circumstances of the eclipse, and "Description of the DAIRCHEM Computer Code" briefly describes the DAIRCHEM computer code. Under "Comparisons of DAIRCHEM with the 1966 Eclipse Data Base...," the ionizing source functions are incorporated into the DAIRCHEM code and the predicted ion and electron densities are compared with the experimental data.

IONOSPHERIC MEASUREMENTS

Data Sources

Many ionospheric measurements were made in Brazil and in other South American countries on the path of totality of the 1966 eclipse. The larger portion of these measurements, however, were made individually and not in coordination with other ground, aircraft, or rocket launched experiments, and hence are of only nominal value to the present analysis. The Defense Nuclear Agency (DNA) (formerly Defense Atomic Support Agency) supported experiments, plus those of National Aeronautics and Space Administration (NASA) and local Brazilian experimenters which were carried out in the vicinity of the Rio Grande rocket launch complex, were closely coordinated with one another and will provide the major fraction of the data which will be described and summarized in this section. The experiments which are considered in detail here are summarized in tables 1 and 2.

Three classes of data exist: ground-based and aircraft-based measurements of electron density versus altitude which are derived from analyses of propagation effects; in-situ measurements of electron density, positive ion density and species composition, and electron temperature which were carried on rocket-launched probes; and rocket-to-ground propagation experiments which yielded altitude profiles of electron density. In this portion, the authors take advantage of the redundancy available in the electron density data to attempt to provide a best-fit to the time and altitude variations of electron density during the eclipse. Because different measurement techniques have different analytical and empirical sources of error, a combination of two or more sources of data should in principle yield results which are more truly representative of the D-region during the eclipse.

Eclipse Coordinate System

The principal difficulty in combining data from ground, aircraft, and rocket-based measurement platforms is the accurate specification of their location with respect to a common eclipse oriented coordinate system. To provide the common coordinate system required, a system utilizing the fewest number of independent variables possible was chosen. The significant variables are altitude, eclipse time, and the duration of totality at the chosen altitude. Eclipse time is specified as seconds before second contact or seconds after third contact for measurements outside totality, or as seconds after second contact and duration of totality for measurements within totality.

The locations of the trajectories of several DNA and NASA sponsored rockets within the altitude-time coordinate system are plotted in fig. 1. Trajectory information for the NASA rockets in this coordinate system was taken from Mechtly et al. [4]. This coordinate system allows one to avoid the problem of location of the data in horizontal coordinates at a given altitude within the eclipse totality because the pertinent coordinates are time after second contact and the duration of

TABLE 1. ROCKET PROBE MEASUREMENTS OF ELECTRON AND ION DENSITY

Rocket Numbers	Instruments	Altitude Range (for data) (km)	Time (UT)	Fractional Obscuration
D 4 Certification	SWIPE*	70 - 110	5 Nov 1355 UT	0.0
D 4	LP**		12 Nov 1354:00	0.8
D 11	LP		12 Nov 1408:37	T
D 13	LP		12 Nov 1422:30	0.8
D 16 Certification	Blunt probe	50 - 80	5 Nov 1535 UT	0.0
D 3	LP		12 Nov 1338:00	.43
D 10	LF propagation		12 Nov 1407:30	T
D 16	LF propagation		12 Nov 1535:00	0.0
N 5	LP	60 - 160	12 Nov 1406:00	0.9
N 9	HF propagation		12 Nov 1408:00	T
N 12	HF propagation		12 Nov 1410:00	0.9
N 19	HF propagation		12 Nov 1500:00	0.3

*SWIPE - Standing wave impedance probe

**LP - Langmuir probe

TABLE 2. GROUND-BASED IONOSPHERIC MEASUREMENTS ON THE 1966 SOLAR ECLIPSE

Measurement	Instrumentation	Location	Comments
Group path (vertical incidence)	HF ionosonde	Cassino	Electron density above 100 km could be determined.
Phase path and absorption (oblique incidence)	HF phase sounder	Bage-Cassino	Phase path and amplitude data on three frequencies.
Absorption	HF riometers	Cassino	Data can be used to verify D-region electron density models.
Group path and absorption	HF airborne ionosonde	East of Cassino	Data can be used to verify D-region and E-region models.
Partial reflection	HF sounder	Cassino	Direct measurements of D-region electron density variation.
Phase path and amplitude (vertical and oblique incidence)	VLF multiple frequency sounder	Pinheiro Maechado	Electron density variation in lower D-region may be inferred from data.

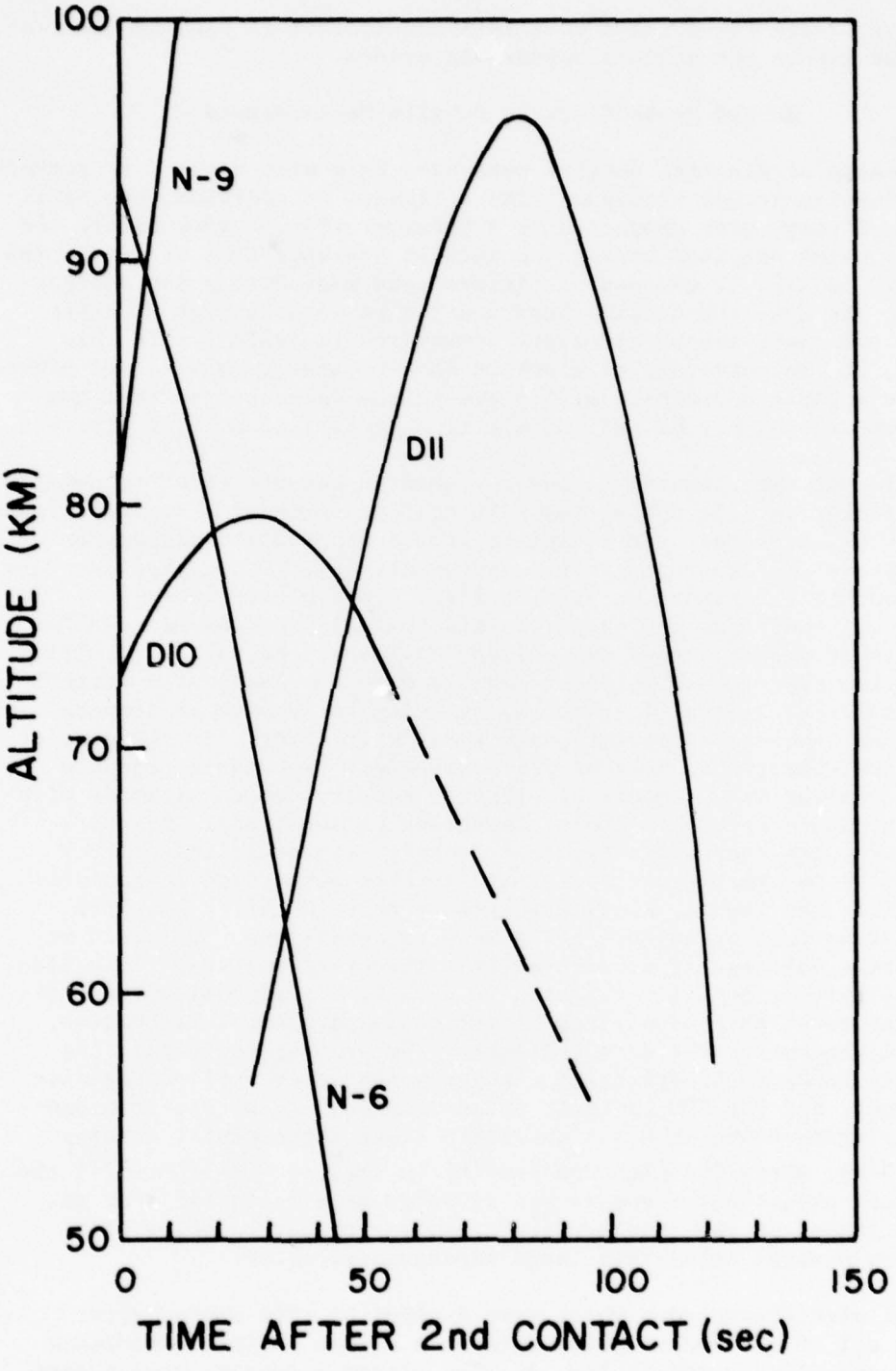

Figure 1. Trajectories of rockets passing through totality expressed in eclipse time coordinates.

totality. Sears [3] gives a more detailed account of placing the trajectories within the eclipse coordinate system.

Rocket Probe Electron Density Measurements

Measurements of electron density were made by a wide variety of rocketborne, in-situ probes throughout the eclipse. In addition, two certification firings were conducted on 5 November 1966, a week before the eclipse, which obtained background data at the same time of day as the eclipse. In all, 12 successful firings were made during the eclipse period. The electron density instrumentation capabilities of these rockets and their launch times are summarized in table 1. In this section, the measurements of electron density are summarized and placed into the eclipse coordinate system previously described so that temporal comparisons may be made of electron density at a given altitude.

The different experimental techniques used to measure electron density from a rocket vehicle during the 1966 eclipse include: Langmuir probes, subsonic blunt probes, and rocket-to-ground propagation measurements to calibrate the Langmuir probe measurements [4]. Other experimenters used absolute laboratory calibrations for probe measurements [5]. In each case, conditions may exist wherein the calibrations adopted for the Langmuir probes during the eclipse may be erroneous. In addition, propagation experiments which are analyzed on the basis of a strictly horizontally stratified ionosphere, ignoring horizontal or temporal variations in electron density, may also be in error. In the case of noneclipse conditions, most of the measurement techniques produced closely similar measurements of electron density versus altitude within the probable errors in their respective calibrations. Figure 2 illustrates the background electron density versus altitude curves obtained by the variety of rocketborne probes summarized in table 1. As shown in the figure, most measurements above about 70 km agree within 20 percent or so for the background conditions. Below 70 km, blunt probe data appear to diverge from the other results. This discrepancy has not been investigated in detail. To emphasize the positive aspects of this comparison of various experimental techniques, the NASA Langmuir probe data (calibrated by propagation data), the Ballistic Research Laboratories (BRL) low frequency (LF) propagation experiment, and the BRL Langmuir probe measurements of electron density all agree above about 65 km within their experimental errors. Below 65 km, where the electron density is smaller than 100 cm^{-3}, the individual experimental errors are as large as a factor of 3 or so, thus estimates of the absolute electron density curves below this level may possess relatively large experimental error.

The most significant data which were derived by this study, after putting all of the rocket probe data on a common eclipse coordinate system, are illustrated in fig. 3. The electron density versus time measurements at selected altitudes between 70 and 90 km are depicted, utilizing all of the available rocket probe and rocket-to-ground propagation data. Three significant features are to be noted in this

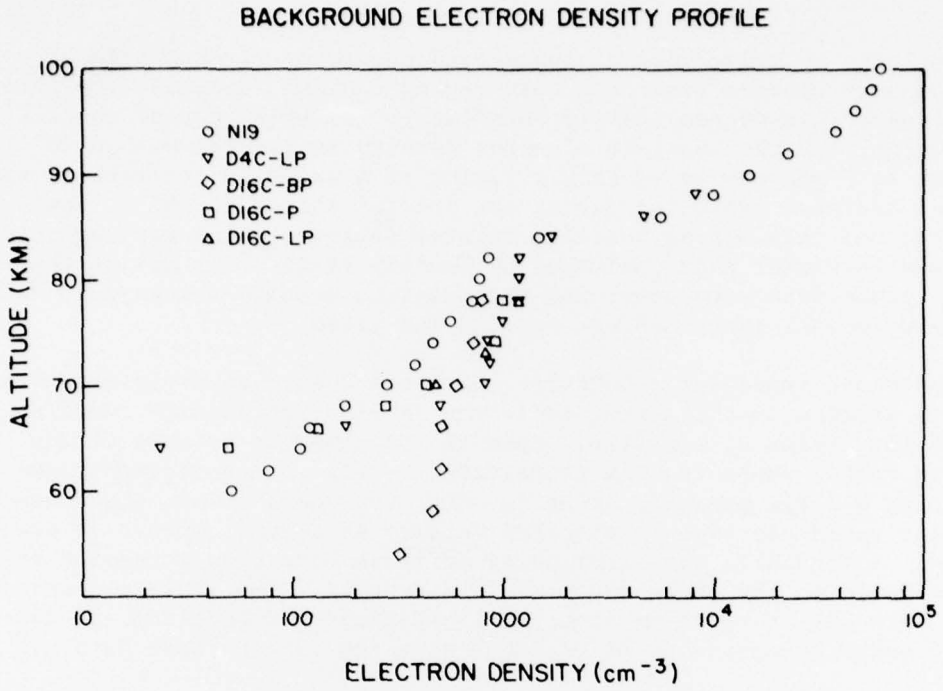

Figure 2. Background measurements of electron density versus altitude from in-situ rocket probes. LP=Langmuir probe, BP=Blunt probe, and P=rocket-to-ground propagation experiment.

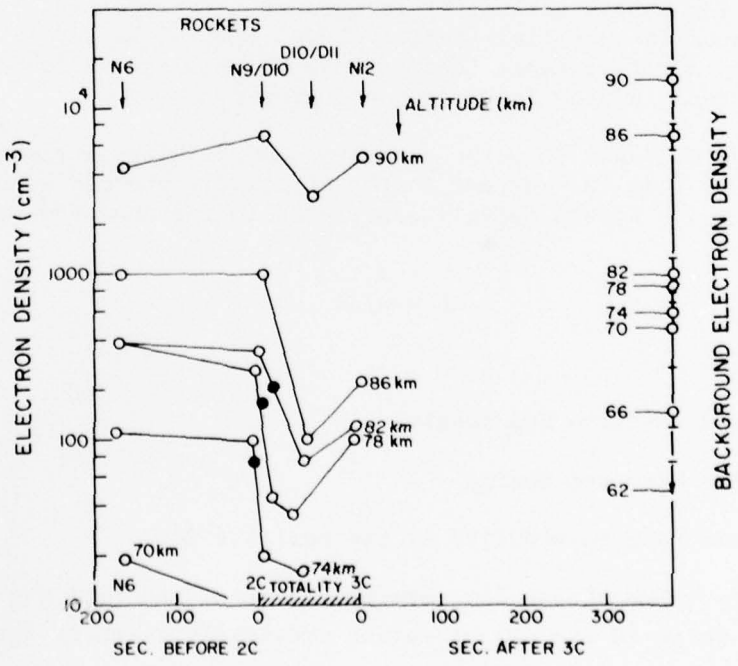

Figure 3. Electron density versus time about totality.

figure: the relative rate of change and magnitude of change in electron density between first and near second contact is small, the rate of decrease in electron density immediately following second contact is very large, and the absolute electron density is reduced within 20 seconds to 2 minutes by roughly a factor of 4 to 10 in contrast to the gradual decrease exhibited during the initial stages of the eclipse. To bring out this strong totality related feature, which was suggested by the NASA rocket data published by Mechtly et al. [4], all of the rocket probe data were used, and the electron density values were taken as the principal experimenters results indicated.

The important ionospheric behavior which has been explicitly demonstrated in this section is the strong reduction in electron density immediately around the region of totality. Even if the intercomparisons of the various rocket probe results illustrated by fig. 3 are de-emphasized by assigning a large probable error to each probe data point, the characteristic rapid decrease in electron density at second contact is preserved. Ionospheric data from other eclipses have also suggested this effect [6,7] in the 70 to 90 km altitude regime. The implications of these data with respect to atmospheric deionization modeling are discussed under "Comparisons of DAIRCHEM with the 1966 Eclipse Data..."

Positive Ion Density Data

Positive ion density and species were measured by in-situ rocket probes over the altitude range of 50 to 100 km. Three types of probes were used: a parachute deployed blunt probe to measure total positive ion density below about 80 km [8], a retarding potential analyzer [9], and a positive ion mass spectrometer to measure total positive ion density and ionic species mass distribution above about 70 km [10,11]. A small common altitude range (about 70 to 80 km) was available to both the blunt probe and the ion mass spectrometer.

As described by Baker [8], the positive conductivity of the ionosphere is determined from the current to the negatively charged blunt probe. The positive ion number density is related to the measured conductivity σ by:

$$N = \sigma/\mu e$$

where

N is the positive ion density

e is the electron charge

μ is the reduced mobility of the positive ion.

The mobility value chosen for interpretation of the data was $\mu = 1.8$ $cm^2V^{-1}s^{-1}$, which is typical of values previously measured for the O_2^+

ion. However, as Narcisi's mass spectrometer measurements showed, the principal positive ion is $H_3O^+(H_2O)$, or higher hydrates, below 80 km or so, the mobility of which is taken as 2.8. When this increased mobility value is used, the positive ion densities reported for the blunt probe experiment are somewhat reduced. A summary of the adjusted blunt probe data and the combined retarding potential analyzer (RPA) and ion mass spectrometer total ion density data is contained in fig. 4. Above 85 km, the positive ion mass spectrometer results were normalized against the RPA total ion density data; hence only a single curve is given for these combined data for each rocket shot. Attempts to normalize the ion mass spectrometer data against the blunt probe ion density data at comparable times during the eclipse were unsuccessful. This lack of success is to be expected insofar as the negative ion densities and the negative ion to electron density ratio do not remain constant during the eclipse at a given altitude.

The positive ion species in the D- and E-regions were measured by Narcisi et al. [10,11]. These data are illustrated in figs. 5a and 5b. Although it is difficult for the authors to assess the physical reality of the very rapid composition charges versus altitude, these data are a useful input to verification of the DAIRCHEM code. In the D-region, rocket velocity may have been large enough to cause breakup of complicated hydrated species in the nosetip shockwave; however, the relative changes in composition between simple and hydrated species are instructive. The total positive ion density data in fig. 4 are the result of smoothing and fitting the three sources of data.

Ground-Based Ionospheric Measurements

During the 1966 solar eclipse, a wide variety of ground-based ionospheric experiments were conducted in South America. The measurements which are of principal interest to this study are propagation measurements from which the electron density versus altitude and time variation can be derived directly. Other measurements provided indirect measurements of D-region electron density variations. The data used in the present study are from measurements summarized in table 2.

The temporal and spatial variation of electron density in the D-region over the altitude range from about 70 to 100 km was obtained by von Biel [12] from analysis of partial reflection data. The partial reflection data provide a continuous record of the electron density throughout the eclipse, which complements the rocket probe data obtained at discrete intervals. The principal disadvantage of the partial reflection sounder technique is the temporal averaging of the signal which is required to obtain reasonable accuracy in the electron density value. For the eclipse, the averaging time constant was 4 minutes, which effectively precludes precise, time-resolved, electron-density measurements immediately around totality where the electron density changes significantly within the averaging interval. Thus, these data are used to define the long-term behavior of electron density in the D-region to cross-calibrate the rocket probe data.

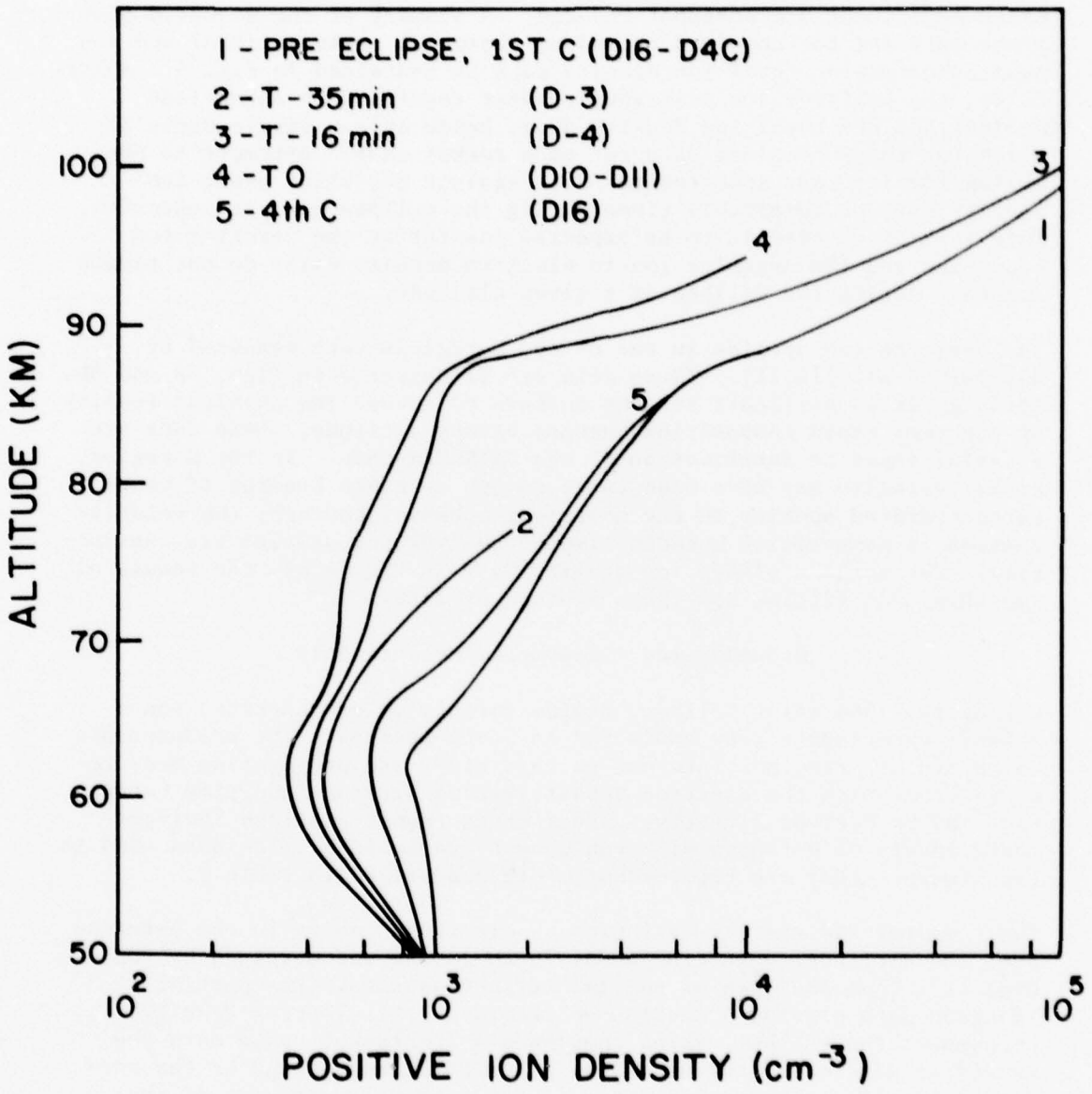

Figure 4. Total positive ion density versus altitude for several times during the eclipse.

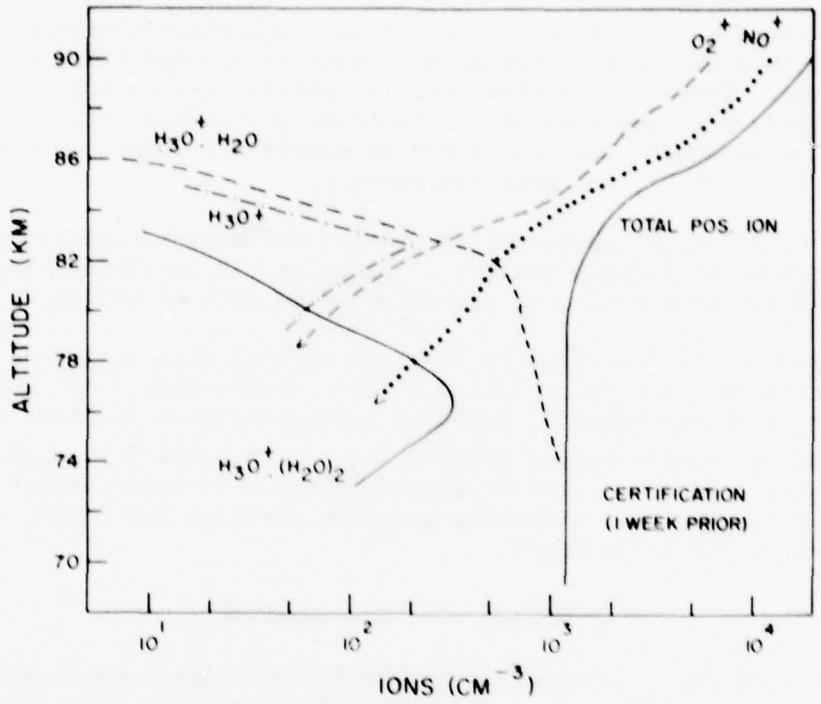

Figure 5a. Positive ion densities measured one week prior to the eclipse (after Narcisi et al., 1972).

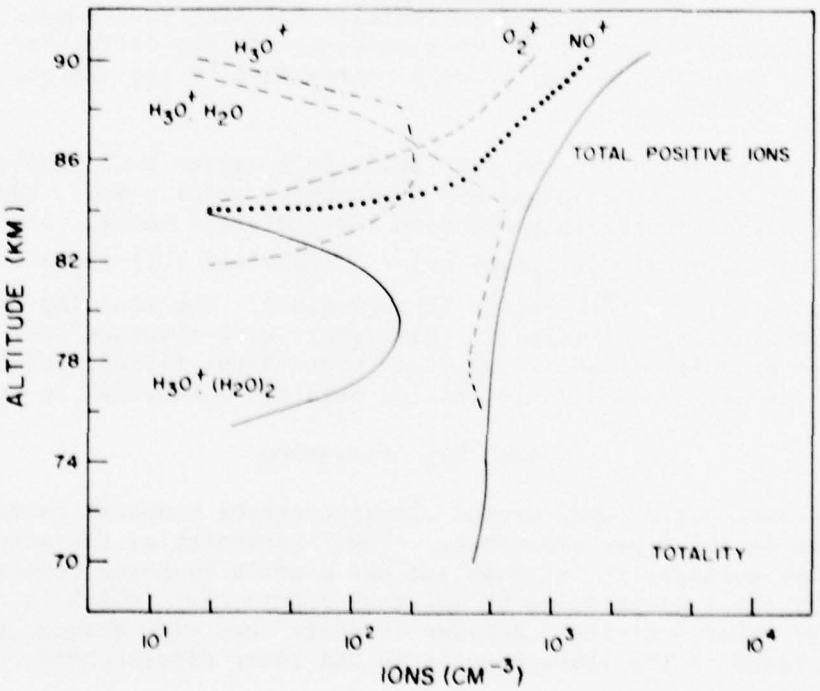

Figure 5b. Positive ion densities measured during totality (after Narcisi et al., 1972).

Figure 6 shows a comparison of the partial reflection electron density data with in-situ rocket probe measurements at several times during the eclipse. These curves show that the partial reflection results agree closely with the rocketborne Langmuir probe data obtained by BRL, Air Force Geophysics Laboratory (formerly Air Force Cambridge Research Laboratory), and NASA instruments.

The good quantitative agreement of partial reflection sounder and rocket probes utilizing a variety of experimental techniques must be considered as verification of the accuracy of each technique.

Examination of the ground-based electron density data indicates that such experiments have two valuable roles: cross-calibration and enhancement of rocket-based N_e profiles versus altitude and time by direct sounder measurements; and provision of a basis for comparison of eclipse D-region qualitative phenomenology with prior efforts using indirect techniques for inferring D-region electron densities, e.g., riometers and VLF/LF sounders.

D-REGION IONIZING SOURCES

Maintenance of the ionization in the daylit D-region between about 50 and 90 km requires several sources of ionization. The intensity of each source has its particular dependence upon temporal, geographical, solar cycle, altitude, and other variables each of which must be quantitatively specified for the circumstances of the 1966 eclipse. Additionally, the eclipse obscuration function for each source must be defined as appropriate. The obscuration functions may differ for each source, and none of them may be well-represented by the visible obscuration function.

Sources of ionization for the 1966 eclipsed D-region are: galactic cosmic rays, solar Lyman-alpha and Lyman-beta, solar x-rays, and energetic electrons precipitated from the radiation belts. The effects of photoionization of $O_2(^1\Delta_g)$ by solar ultraviolet (UV) radiation were also considered, but this source is negligible. The ionizing sources for the 1966 eclipse utilized in this report were obtained from measurements, for example, of solar x-ray and Lyman-alpha fluxes, and from models. The sources and their related data are summarized in table 3.

Cosmic Ray Ionization

Galactic cosmic rays (GCR) are an almost constant temporal source of ionization in the upper atmosphere. Their intensity at the earth varies with geomagnetic latitude and has a small temporal modulation imposed by the average value of solar wind intensity, which is controlled by solar activity. Because of their very high energy, their stopping range in the atmosphere is in the lower stratosphere, and

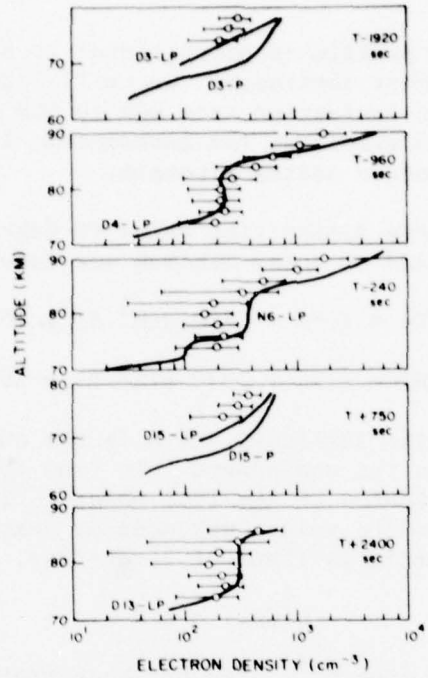

Figure 6. Comparison of partial reflection data with in-situ rocket probe electron density measurements.

TABLE 3. IONIZATION SOURCE FUNCTION EXPERIMENTAL DATA

Ionizing Radiation	Measurement	Experimenter [reference]
Lyman alpha	Rocket photometer	Blamont and Malique [25]
Lyman alpha	Rocket photometer	Accardo [26]
X-rays	Rocket spectrometer	Argo et al. [14]
X-rays	Rocket photographs	Underwood et al. [34]
X-rays	Satellite photometer	Solar Geophysical Data [47]
X-rays	Rocket photometer	Accardo [26]
Galactic cosmic rays	No direct measurement	
Solar Lyman beta	No direct measurement	
Solar UV (photo-detachment)	No direct measurement	
Energetic electrons	No direct measurement	Indirect estimate from Pfitzer and Winckler [20]

hence their ionization profile is proportional to atmospheric neutral particle density at higher altitudes. Heaps [13] outlines the derivation of the ionospheric ionization rate due to GCR and presents an empirical formula which describes the geomagnetic latitude and altitude variation of the ionization source strength.

The GCR ionization source intensities below 60 degrees magnetic latitude at solar maximum and at solar minimum are described by:

$$Q(\text{GCR: S.MAX}) = (174 + 1930 \sin^4 \Lambda) \times 10^{-20} N$$

$$Q(\text{GCR: S.MIN}) = (174 + 2840 \sin^4 \Lambda) \times 10^{-20} N$$

where Λ is the geomagnetic latitude, and N is the number density (cm^{-3}) of neutral particles in the atmosphere. To find the GCR ionization source for the circumstances of the 1966 solar eclipse, an interpolation between these bounding values was made as described in Heaps [13]. For 1966, at a geomagnetic latitude of 24 degrees,

$$Q(\text{GCR}) = K N$$

where $K = 2.32 \times 10^{-18}$ ions s^{-1}. The altitude profile of the cosmic ray ionization source is illustrated in fig. 7.

Precipitating Electrons

A number of experimental observations and theoretical factors suggest that precipitating electrons introduced a temporally constant source of ionization in the D-region during the eclipse. Evidence of trapped or precipitating electrons was obtained by rocketborne x-ray counters which observed anomalously high counting rates from about 160 km altitude to near apogee both before and during the eclipse [14]. Absorption measurements made during totality suggest that the D-region electron density is anomalously high at this time, which could only result from either an unknown source of detachment of electrons from negative ions or from an added ionization source [15]. Balloonborne x-ray detectors flown in this region have detected bremsstrahlung from precipitated energetic electrons [16]. In addition, Potemra and Zmuda [17] showed that electron precipitation at midlatitudes could contribute a significant nighttime ionization source to the D-region. In view of the eclipse experiment location on the western portion of the South Atlantic geomagnetic anomaly, the possibility of electron precipitation from the lower trapped radiation belt must be accounted for.

Eather and O'Brien [18] attempted to detect electron precipitation in this geographical region in 1967 by photometric methods but did not detect any 4278-angstrom band emission enhancements caused by electron ionization and excitation, $N_2 + e \rightarrow N_2^+* + 2e$, within their instrumentation sensitivity limits of 0.2 Rayleighs. From these observations, they concluded that the particle precipitation over the region

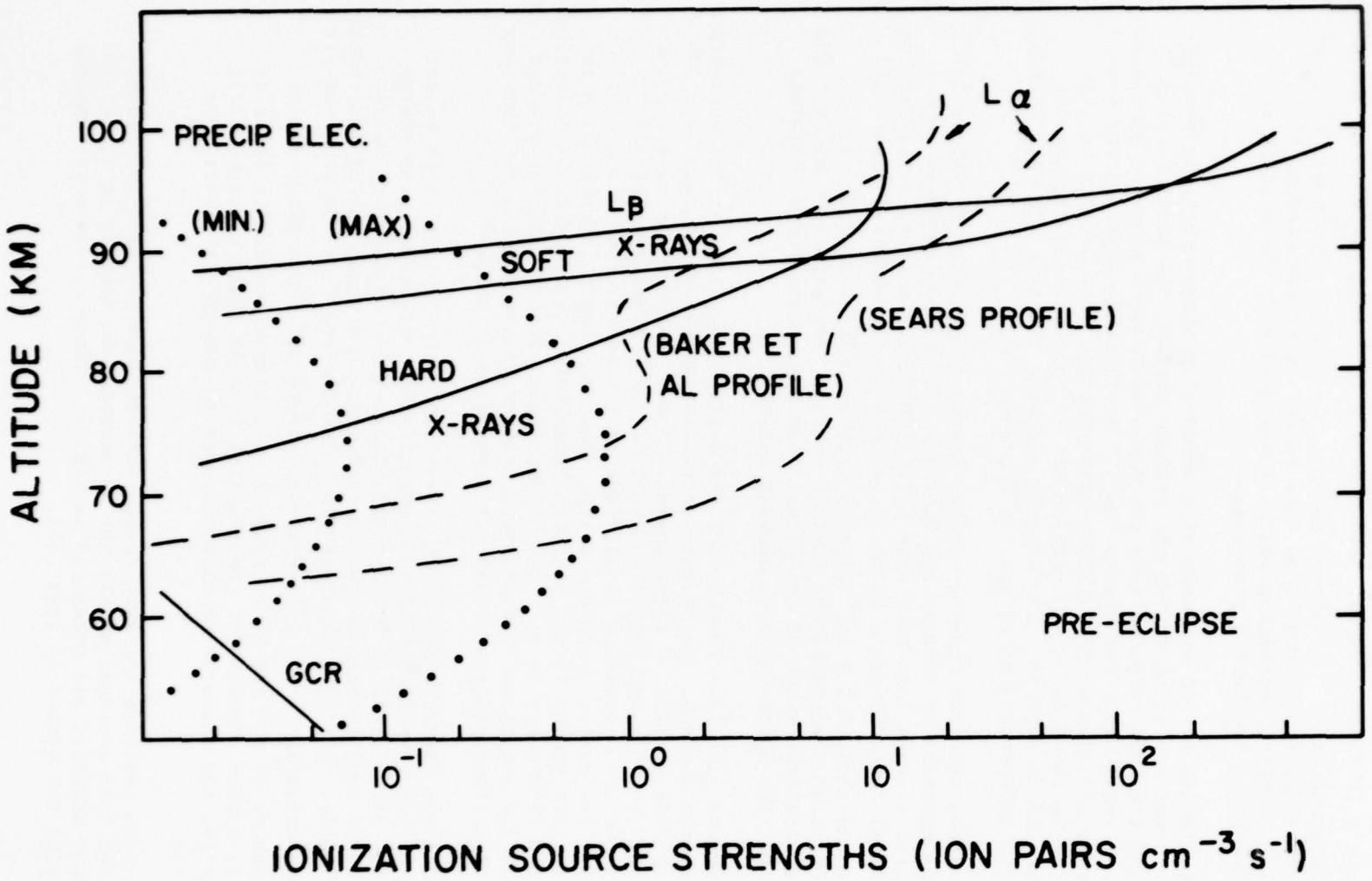

Figure 7. Altitude dependence of the ionizing sources for the 12 November 1966 solar eclipse - pre-eclipse conditions

accessible to their view was less than 7×10^{-4} ergs $cm^{-2}s^{-1}$, or about 10^4 electrons $cm^{-2}s^{-1}$ of 50 keV energy. As Potemra and Zmuda point out, electron fluxes much lower than this energy limit are capable of creating D-region ionization which is measurable in the absence of normal daytime ionization processes.

In the absence of any evidence of a temporally unique particle precipitation event occurring during the eclipse period, the precipitating electron flux was computed from the measured trapped electron population on the L-shell which intersects the 100 km altitude level in the geographical location of the eclipse measurements. The L-value at this location is about 1.2 which corresponds to an invariant geomagnetic latitude of 24 degrees. The average electron lifetime for this L-shell, which is independent of energy, is 250 days [19].

The trapped electron flux in several energy ranges from 50 keV to 1.7 MeV was measured by Pfitzer and Winckler [20] on 30 September 1966. Given the average loss rate from this time to the eclipse date, with no additional replenishment, about 88 percent of the observed flux would remain and about 4.1×10^{-8} of this flux would be lost each second. This fraction represents the minimum average precipitated flux over the entire longitude range of the L-shell and hence represents a minimum value for the South Atlantic anomaly region.

Gassman and Pike [21] showed that the eclipse location, on the westward side of the anomaly, can receive precipitating electrons from over 300 longitudinal degrees of the trapping volume. Because the mirror point altitudes for a given magnetic moment of the trapped electrons are lowest and are descending in altitude in the western portion of the anomaly, the entire average electron loss rate may be attributable to loss in this region in the southern hemisphere; hence, the precipitating particle fluxes may be an order of magnitude greater than the average value would indicate. The measured trapped fluxes and the two limiting cases for precipitating fluxes are summarized in table 4.

The altitude distribution of the ionization depends to a large extent upon the energy spectrum of the precipitating particles. The energy spectrum as measured by Pfitzer and Winckler is considerably harder than those sample spectra adopted by Potemra and Zmuda for midlatitudes. For example, the integral energy spectrum derived from the measurements is approximately $F = E_o E^{-1}$; whereas Potemra and Zmuda adopt energy dependences of E^{-3} and E^{-5}. However, the trapped radiation belts do exhibit harder spectra for the electron flux at lower L values [22]; therefore, the measured spectrum is used to compute the ionization profile.

Ionization profiles for both cases, uniform loss averaged over longitude and loss averaged within the westernmost 60 degrees of the South Atlantic anomaly, are presented in fig. 7. These curves were computed following the method of Rees [23].

TABLE 4. TRAPPED AND PRECIPITATING ELECTRON FLUXES AT THE BRAZILIAN ECLIPSE SITE

Energy Range (keV)	Trapped Flux el. cm^{-2} sr^{-1} s^{-1} KeV^{-1}	Precipitating Flux (Longitudinal Average) el. cm^{-2} s^{-1} KeV^{-1}	Anomaly Peak el. cm^{-2} s^{-1} KeV^{-1}
50 - 120	2×10^{5}	5×10^{-2}	5×10^{-1}
120 - 290	9×10^{4}	2×10^{-2}	2×10^{-1}
290 - 690	9×10^{3}	2×10^{-3}	2×10^{-2}
690 - 1700	2×10^{3}	5×10^{-4}	5×10^{-3}

Solar Lyman-Alpha and Lyman-Beta

The solar Lyman-alpha emission intensity is a function of solar activity [24]. Measurements of the solar Lyman-alpha energy flux at times near the eclipse range from 1.35 erg/cm^2 sec to 5.7 ergs/cm^2 sec [25,26]. The upper value is more consistent with that expected for the solar activity level at the time of the eclipse. The lower value may have been produced by ionization chamber window degradation before or during the measurement [25]. For purposes of this work, the 5.7 erg/cm^2 sec value is adopted, which corresponds to a photon flux of 3.0×10^{11} photons cm^{-2} s^{-1}.

The solar Lyman-beta flux is also dependent upon the level of solar activity. Swider [27] adopts a value of 100 for the ratio of Lyman-alpha to Lyman-beta photon fluxes, whereas Tousey [28] reports a ratio of 85 for the respective energy fluxes. No direct measurements of Lyman-beta were made during the eclipse period. In addition to direct Lyman-beta, the continuum near the line also produces a small degree of ionization. Therefore, the equivalent Lyman-beta flux is taken as 3.0×10^9 photons cm^{-2} s^{-1}.

The ionization produced by solar Lyman-alpha and Lyman-beta radiation depends upon the altitude distribution of the NO and O_2 which are the ionized species, respectively. Lyman-alpha is strongly absorbed by O_2; hence the distributions of both neutral species affect the ionizing source strength for Lyman-alpha.

Measurements and theoretical estimates of NO density versus altitude have varied by more than a factor of 10. Original computations of the ionospheric response to the 1966 solar eclipse [3] utilized NO profiles derived from Meira [29]. Measurements by Baker et al. [30] made at White Sands, which is at a corresponding latitude in the northern hemisphere, indicate an overall lower NO density profile with a more pronounced minimum in density near 85 km. A comparison of the ionizing source strength utilizing these two NO profiles is presented in fig. 7, for preeclipse conditions. The figure shows that for the first source strength profile (high NO content) the Lyman-alpha ionization predominates over a much larger altitude range than for the low NO content computation.

Because of the wide differences in empirical and theoretical NO profiles, and their potential effects upon D-region ionization profiles, the single "proper" or optimum profile as an a priori input to our study cannot be arbitrarily selected. Rather, the available data on electron and ion density profiles have been used and an attempt has been made to select the optimum NO profiles based upon an empirical best fit to the ionization data. This procedure is outlined in the section on comparison of the DAIRCHEM code with the 1966 eclipse data base.

The solar Lyman-beta ionization profile is computed in a straightforward manner in the DAIRCHEM code and depends only upon the O_2 neutral density profile and the overall Lyman-beta flux. The ionization source strength versus altitude from solar Lyman-beta is illustrated in fig. 7.

Solar X-Rays

Measurements of the unobscured solar x-ray flux were made from satellites and from rockets launched from the Brazilian eclipse site. These measurements may be divided into two spectral groups according to the region of the ionosphere which they ionize: the hard x-rays between 1 and 10 angstroms are capable of ionizing the D-region below 90 km; the soft x-rays between about 30 and 100 angstroms contribute ionization mainly to the E-region above 90 km. Both groups are important around 90 to 100 km.

The measured unobscured x-ray fluxes in both groups are summarized in table 5. Note that the experimental techniques for determining these fluxes depend upon the x-ray absorption edges of the photometer windows which generally do not coincide with the two bands specified. Therefore, the spectral distribution and total intensity within these bands must be inferred from the data.

The spectral distributions in the two x-ray spectral regions derived by Swider [27] were adopted for the present study. These spectral distributions were normalized to correspond with the more limited bandpass x-ray fluxes measured. In general, details of the spectra derived by Swider and the measurements for the eclipse period were in good agreement, and normalization of the two derived spectra to the measured x-ray fluxes should be accurate to within about 20 percent. Figure 8 compares the observed fluxes and the x-ray spectra in the two wavelength regions adopted for this study.

The ionization profile resulting from absorption of the two solar x-ray emission bands, 1 to 10 angstroms and 31 to 100 angstroms, was computed for the unobscured sun. After normalization for the incident integrated unobscured solar flux in the two bands of interest, the ionization profiles computed were not significantly different from those computed by Swider for a solar zenith angle of 25 degrees. The computed x-ray ionization source strength profiles are illustrated in fig. 7.

Definition of the Eclipse Obscuration Functions

The temporal variation, in addition to the absolute magnitude versus altitude, of the ionizing radiations must be defined during the eclipse. Solar radiation eclipse obscuration functions were defined for solar Lyman-alpha and Lyman-beta, visible and near UV radiation, and both the hard and soft solar x-ray emissions.

Visible and near UV obscurations functions are computed in DAIRCHEM by using the geometrical formula of Rydbeck [31] and the UV limb darkening

TABLE 5. UNOBSCURED X-RAY FLUXES

Wavelength (angstroms)	Flux (ergs/cm^2 sec)	Experiment
0 - 8	2.3×10^{-4}	Solrad 8
8 - 20	1.0×10^{-2}	Solrad 8
44 - 60	1.85×10^{-1}	Solrad 8
33.74	1.4×10^{-2}	Sandia rocket
18.97	2.6×10^{-2}	Sandia rocket
18.63	0.5×10^{-2}	Sandia rocket
16.01	0.24×10^{-2}	Sandia rocket

Solrad data from Solar Geophysical Data [47]
Sandia data from Argo et al. [14]

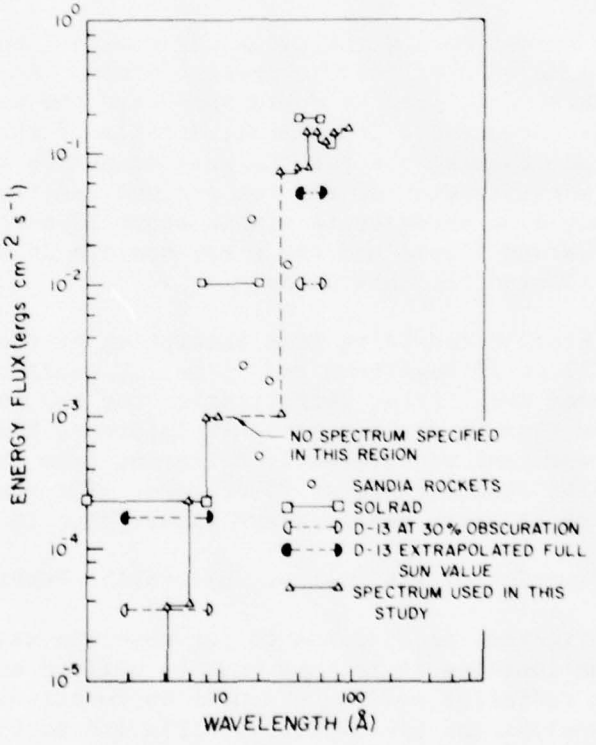

Figure 8. Solar X-ray spectrum for the 1966 solar eclipse.

model of Pierce and Waddell [32]. These obscuration functions are illustrated in fig. 9.

Lyman-alpha and Lyman-beta obscuration functions are somewhat more complex. Before 1958, the flux of Lyman-alpha radiation incident upon the atmosphere within the region of totality was believed to be negligible. During the 1966 solar eclipse, two independent measurements of Lyman-alpha flux within the umbra were made and both showed a residual flux. Measurements made by Blamont and Malique [25] showed solar limb brightening in L_α which extended above the photosphere or optical limb to altitudes greater than 2500 km. A residual L_α flux of 0.14 percent was reported for totality. Bowhill* estimated a residual flux of about 0.5 percent, based upon different data.

Two possible mechanisms may account for residual L_α flux observed at totality: resonant scattering in the uneclipsed and penumbral portions of the terrestrial hydrogen geocorona, and failure to achieve complete totality over the L_α disk. Sears [3] estimated the magnitudes of these respective components as being less than 0.5 percent and about 0.1 percent, respectively. For this study, the residual L_α flux at totality as 0.5 percent was used. The temporal behavior of the L_α ionizing source strength during the eclipse is summarized in fig. 9.

Treatment of the Lyman-beta obscuration function is considerably simpler than for Lyman-alpha because the hydrogen geocorona is much less optically thick. Meier [33] has shown that for near zero solar zenith angle and for exospheric temperatures above about 900 °K, the optical thickness through the geocorona to an altitude of 100 km is less than two. Hence, the requirements for a radiation transport model are considerably lessened. The radiation transport considerations for this obscuration function are neglected and a visible obscuration function as indicated in fig. 4 will provide results of adequate accuracy.

X-Ray Obscuration Function

The x-ray obscuration function depends strongly upon the localized distribution of x-ray sources on the solar disc. An analytical function cannot be derived in general, and experimental data must be sought. Photographs of the solar disc in x-ray wavelengths were obtained by Underwood et al. [34] for the unobscured sun at the time of the solar eclipse. Although it is well-known and strongly evident in the x-ray photographs that the harder portions of the x-ray spectrum are more localized than the soft emission spectrum, thus producing a larger temporal gradient in ionization source strength, this analysis shows that such temporal gradients cannot be resolved adequately by the D-region measurement techniques and the available data. Hence, although

---

*Comments made at the 1966 Solar Eclipse Symposium, Sao Jose dos Campos, Brazil, February 1968.

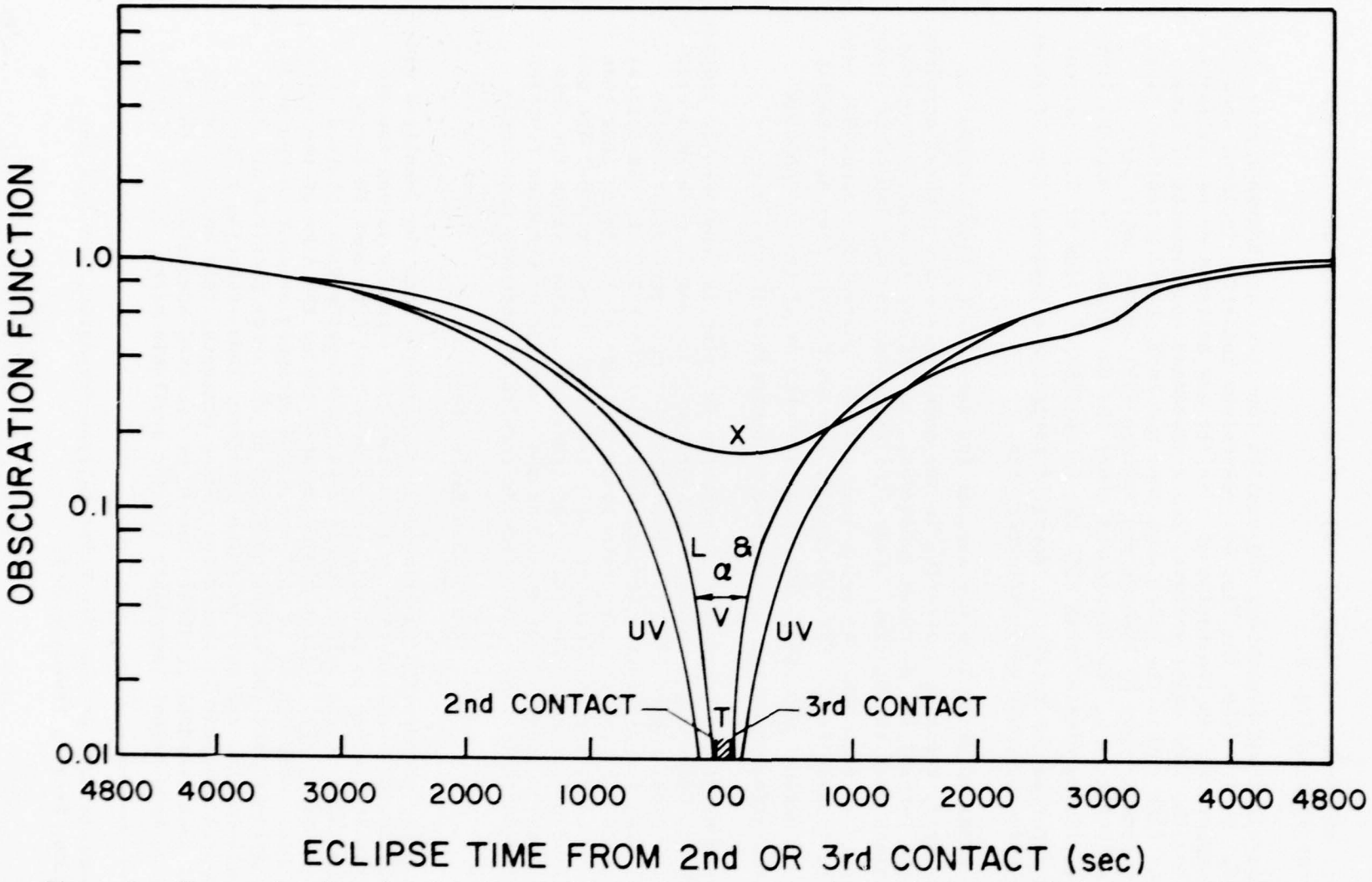

Figure 9. Obscuration function for the visible (V), Lyman-alpha (L_α), ultraviolet (UV), and soft X-ray (X) fluxes for the solar eclipse.

not justified in detail, the soft x-ray obscuration function derived from the 27- to 40-angstrom photograph is used for the entire soft x-ray flux.

Measurements of solar x-rays during the 1970 eclipse by Accardo et al. [35] give residual values of 16 percent during totality for the x-ray band from 44 to 60 angstroms, which is in very good agreement with the obscuration function used here. Measurements in the 2- to 8-angstrom band showed a residual value of 5 percent during totality. Subsequently, the hard x-ray obscuration function used here follows the soft x-ray function down to about 5 minutes before totality and then descends to the lower 5 percent value during totality.

Summary of Ionizing Source Strength and Obscuration Function Calculations

One may conclude from the results of the definition of the ionizing sources, their altitude variations, and eclipse obscuration functions that an adequate description of the ionizing source input to the D-region under eclipse conditions entails a complicated superposition of time and altitude-varying functions. It is instructive to compare the altitude profiles of ionizing source strength during totality in a format equivalent to that used in fig. 7 for preeclipse conditions. Figure 10 illustrates these results. The figure illustrates the importance of the precipitating electron flux over the entire lower D-region compared with the eclipsed solar ionizing sources such as L_α and x-rays. As will be shown later, a significant precipitating electron flux is required to model the ionization profile in preeclipse conditions. As in the preeclipse condition, the galactic cosmic ray ionization is negligible over the altitude range of interest to this study.

DESCRIPTION OF THE DAIRCHEM COMPUTER CODE

DAIRCHEM determines the number density as a function of time at a specified altitude for each of several charged and neutral species. A large set of time-dependent, coupled chemical reaction equations is solved, of the form

$$\frac{dy_i}{dt} = q_i + \Sigma \text{ (rates forming } y_i) - \Sigma \text{ (rates removing } y_i)$$

where y_i is the time-dependent number density of the i^{th} species; q_i is the nonchemical, nonphoton source term; and the last two terms represent formation and removal terms due to chemical and photon reactions. The current reaction set contains 493 reactions, involving 64 neutral, positive, and negative species.

Basic routines for solving these stiff, coupled differential equations have been taken from the existing AIRCHEM atmospheric chemistry code

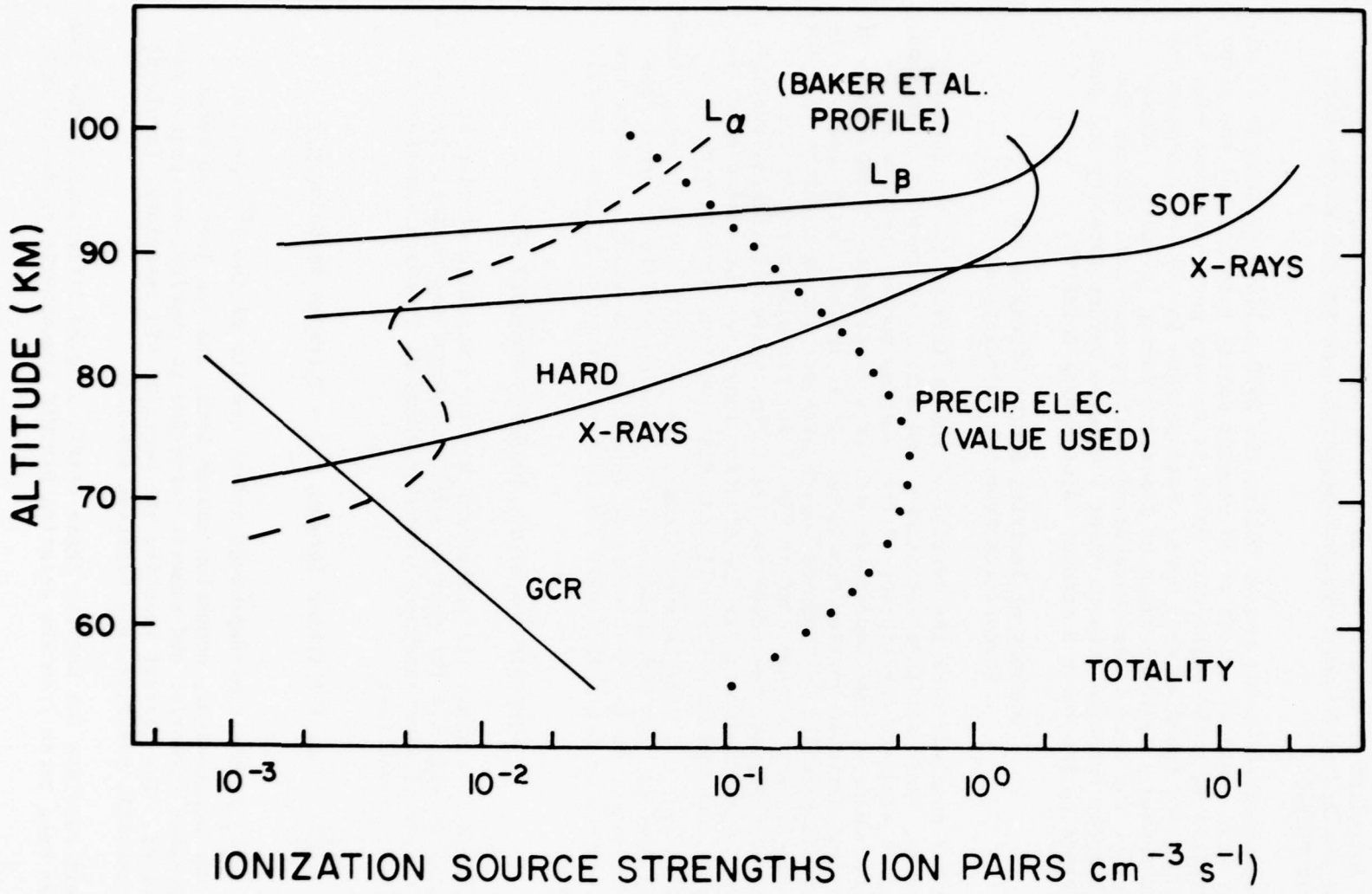

Figure 10. Altitude dependence of ionizing sources for the 12 November 1966 solar eclipse - totality.

[36]. The latest version of the numerical integration routine is based on a predictor-corrector algorithm called the K-method [37,38]. Its improved speed can now simulate a 24-hour period at any mesospheric altitude in less than 2 minutes CPU time on a CDC 7600 computer.

The solar flux arriving at the altitude of interest is determined by taking into account absorption by N_2, O_2, CO_2, and O_3. The column density of each absorbing species is calculated along the geometric straight-line path traveled. Solar zenith angles near and greater than 90 degrees are readily accommodated. Scattering into the volume of interest and away from the line of sight are not presently incorporated. The absorption of solar radiation and dissociation of O_2 in the 175 to 210 nm spectral region dominated by the Schumann-Runge bands are handled by using the semiempirical method of Kockarts [39]. When a solar eclipse is in progress, the incident solar flux is first reduced by the appropriate obscuration functions for the visible, UV, Lyman-alpha, and soft and hard x-ray portions of the spectrum.

Photodetachment of electrons from negative ions, and also photodissociation of ions and neutrals are considered, and the appropriate cross sections have been taken from the literature and sponsored research work (e.g., Vanderhoff [40], Vanderhoff and Beyer [41], Cosby et al. [42] and references contained therein). In practice, chemical means of detaching electrons from negative ions are found to dominate the photodetachment processes [43].

A more detailed description of the DAIRCHEM computer code as it is used in the current set of runs may be found in Hoock and Heaps [44].

COMPARISONS OF DAIRCHEM WITH THE 1966 ECLIPSE DATA BASE PREECLIPSE CONDITIONS

DAIRCHEM runs were made at altitudes between 60 and 90 km to develop profiles of electron and total positive ion densities to compare with experimental measurements. To accurately simulate the altitude profiles of electron densities during uneclipsed conditions, the precipitating electron ionization source previously described had to be included. The magnitude of this source of ionization was determined by comparing code results at 60 and 66 km with measured electron densities. The results of this procedure showed that the magnitude of the precipitating electron ionization source was the maximum value modeled (fig. 7). Above 66 km, the solar Lyman-alpha ionizing source becomes increasingly important, depending in magnitude and profile upon the NO model chosen. The effects of varying the NO density profile modes were illustrated in fig. 7. Best fit of the code predictions to the measured electron densities over the 70 to 80 km altitude range occurred when the Baker et al. [29] profile was chosen, although a fairly wide variation of NO densities in this region can be accommodated. Figure 11 illustrates the simulated and experimentally determined electron and total positive ion altitude profiles for preeclipse conditions.

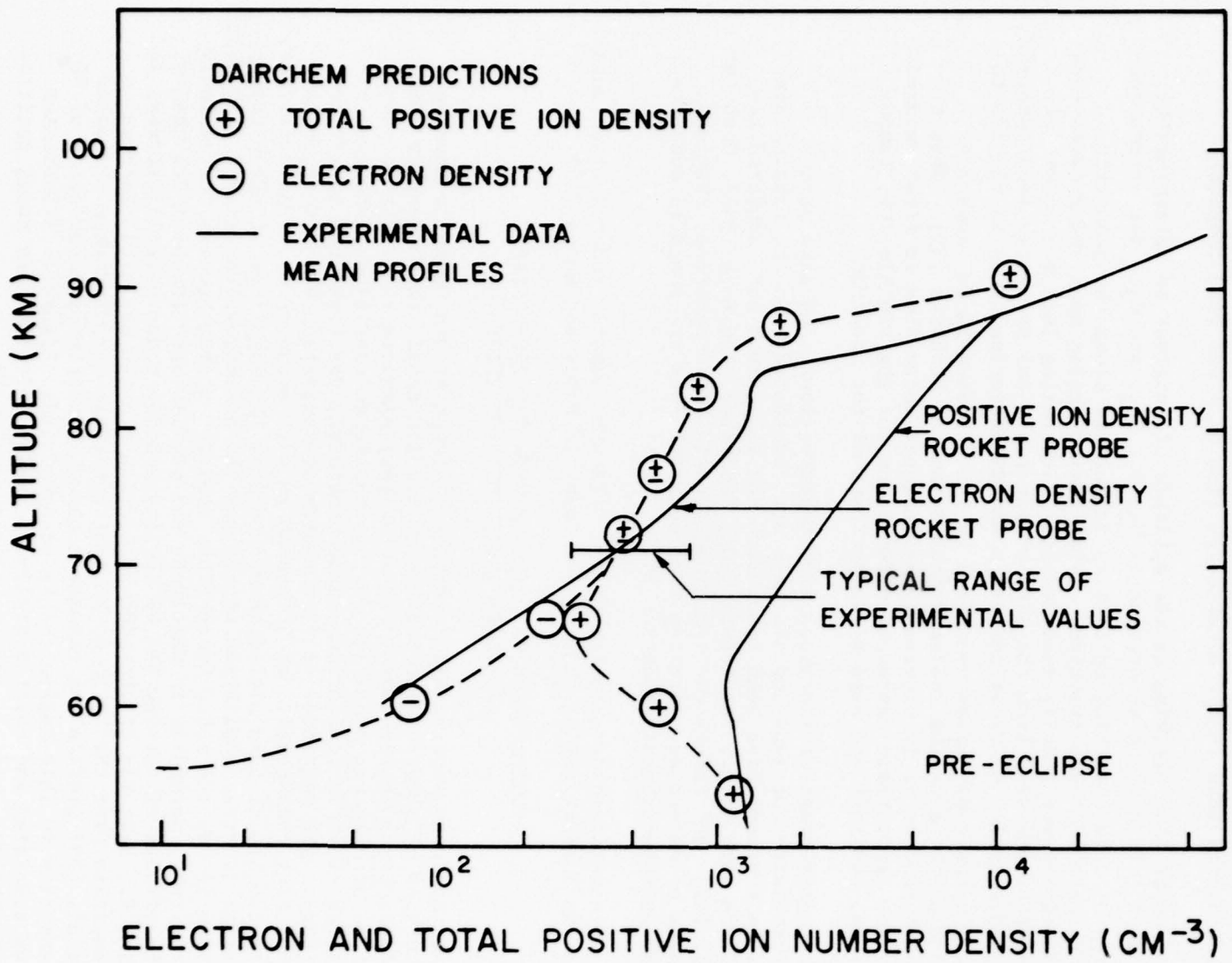

Figure 11. Electron density and total positive ion density during pre-eclipse conditions are compared for DAIRCHEM predictions and rocket probe data.

While the electron density profiles are in reasonable agreement over the entire altitude range, the code predicts substantially lower values of total positive ion density than were observed over the 60 and 85 km interval. The figure shows that significant negative ion densities may be inferred as high as 90 km from the data, whereas the code predicts very low negative ion densities above about 70 km. A somewhat different picture emerges if the total positive ion density curves of Narcisi et al. [10] are used (figs. 5a and 5b). The figures show that the uneclipsed positive ion density remains almost constant at about 1×10^3 cm^{-3} between 72 and 84 km and follows the electron density curve above 82 km. These data imply a negative ion cutoff at 82 km; however, the accuracy of the total positive ion profile below about 90 km, which is inferred from the ion mass spectrometer measurements, is subject to some uncertainty. Hence, a quantitative discrepancy between code simulation and observational data remains with respect to total positive ion density and inferred negative ion density in the 60 to 85 km region.

Identification of Positive Ion Species

The positive ion species measured by mass spectrometer probes [10] before and during the eclipse may be compared with DAIRCHEM predictions. Figures 5a and 5b illustrate the measured positive ion species profiles for a certification round, several days prior to the eclipse and at totality. The figures show that, without regard to the magnitude of the total positive ion density, at higher altitudes the NO^+ and O_2^+ species predominate throughout the eclipse, whereas below about 82 to 84 km, hydrated species predominate.

DAIRCHEM simulations of positive ion densities for preeclipse and totality conditions, shown in figs. 12a and 12b, correctly give the observed NO^+ and O_2^+ predominance at higher altitudes. The simulated O_2^+ component is somewhat suppressed, indicating that the hard x-ray flux or flux of precipitating electrons of approximately 40 keV energy may have been underestimated. DAIRCHEM predicts that the first hydrate of NO^+ is a major ion in the 80 to 86 km region, particularly during totality, but $NO^+ \cdot H_2O$ was detected on only one flight made at 80 percent obscuration (not shown). Two possibilities for the discrepancy are that the rate along the hydration chain is too high (temperature and water vapor content were not measured), and that the hydrated ions were broken up by passage through the probe shock wave or by wall effects, thus appearing as NO^+. Better qualitative agreement is obtained between measured and simulated NO^+ profiles if the simulated NO^+ and $NO^+ \cdot H_2O$ are added together.

At altitudes below the NO^+ region, hydronium hydrates, $H_3O^+ \cdot (H_2O)_n$, predominate both before and during the eclipse. The data show that masses 37 and 55 (n = 1 and 2) predominate, whereas DAIRCHEM predicts

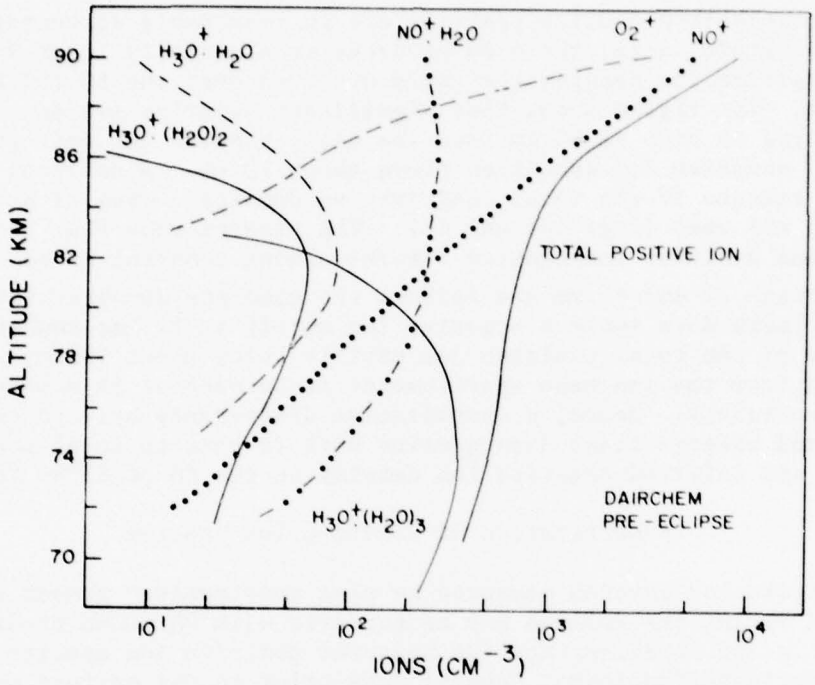

Figure 12a. The DAIRCHEM simulation of positive ion densities for pre-eclipse conditions.

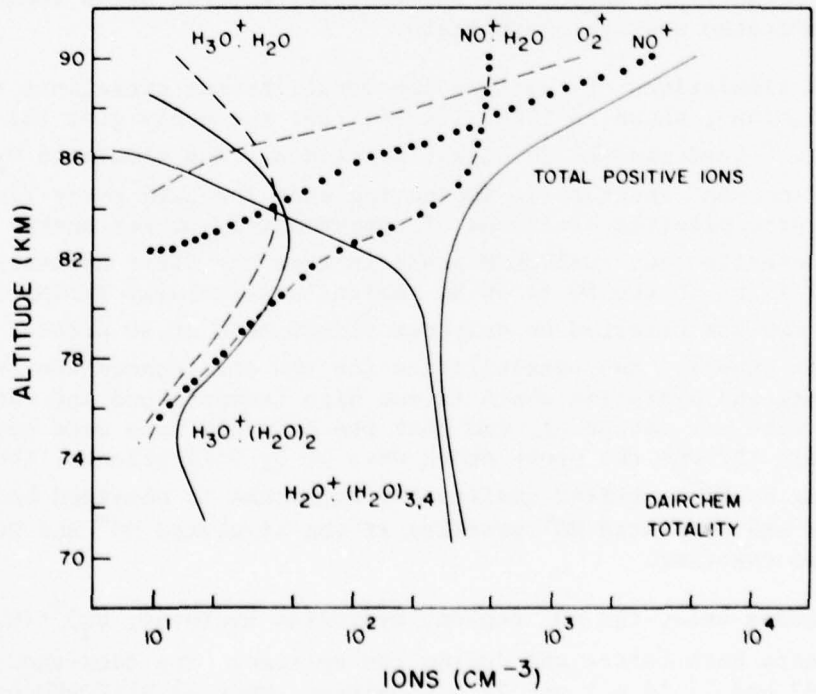

Figure 12b. The DAIRCHEM simulation of positive ion densities during totality.

that higher hydrates are relatively more important. Moreover, as totality is approached, the lower hydrates tend to grow into the higher hydrates; the total ion concentration remains reasonably constant. The authors believe that the DAIRCHEM predictions are consistent with the data insofar as the rapid passage of the ion mass spectrometer payload through the lower D-region, at supersonic velocities, will tend to dissociate the weakly bound multiple hydrated species. Hence, hydrated ions of mass 55, 73, or greater may be observed as lower hydrates, 55, 37, or 19.

The major differences then between the simulated and measured positive ion densities are the quantitative failure of the code to yield the large total positive ion densities which were inferred from rocket probe measurements and the tendency of the code to predict higher hydrates of NO^+ and H_3O^+ than were measured.

Temporal Variations of Electron Density

One of the major reasons for undertaking the detailed comparison of DAIRCHEM with the 1966 solar eclipse experiment is to model the very rapid changes of electron density observed to occur immediately at second contact. Previous ground-based measurements reported by Sears [7,45] had indicated that there were rapid and large changes in D-region electron density associated with the totality region which appeared to be greater in magnitude than could be easily explained by lumped parameter reaction rate codes.

The temporal changes in electron density measured by the several rocket flights within a few hundred seconds of totality were illustrated in fig. 3. The figure shows a reduction of electron density of a factor of 3 to 10 within a few tens of seconds or less at second contact. The figure also shows a clear-cut and rapid decline in electron density at second contact based not only upon the combined data but also upon comparison of measurements made within individual groups. Further, the cross-calibration of rocket probe results with each other, and with ground-based electron density measurements, shows that the observed density decrease is much greater than the experimental errors inherent in the individual measurement technique.

The attempt of the DAIRCHEM code to adequately simulate the rapidity and magnitude of the electron density decrease at second contact is illustrated in fig. 13. The inability of the code to produce any rapid drop in electron density above 70 km during totality is apparent.

To determine the reason for the computer code's failure to simulate the rapid changes in electron density about totality, a closer look at the negative ion chemistry must be taken. A schematic chart of the flow of charge between electrons and negative ions is illustrated in fig. 14, with a more detailed listing of pertinent reactions given in table 6.

The most rapid electron loss process is the three-body attachment to O_2. After O_2^- is formed, further reactions carry the negative charge down

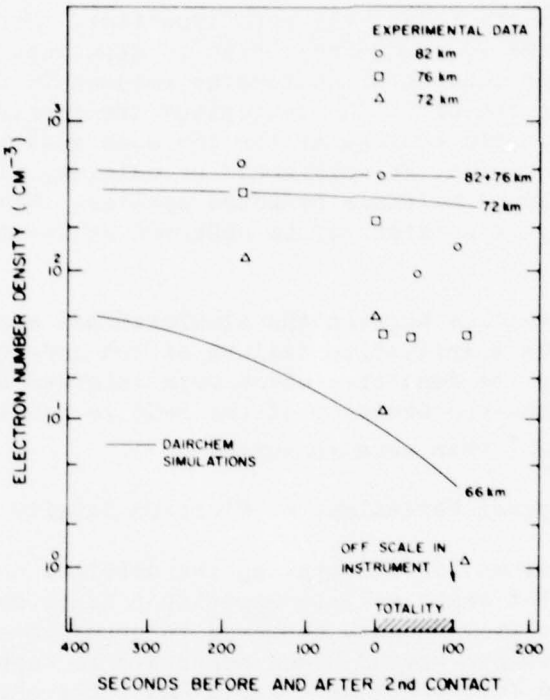

Figure 13. Variations of electron density versus time near 2nd contact. Data points from rockets are indicated by symbols. DAIRCHEM simulations are solid line.

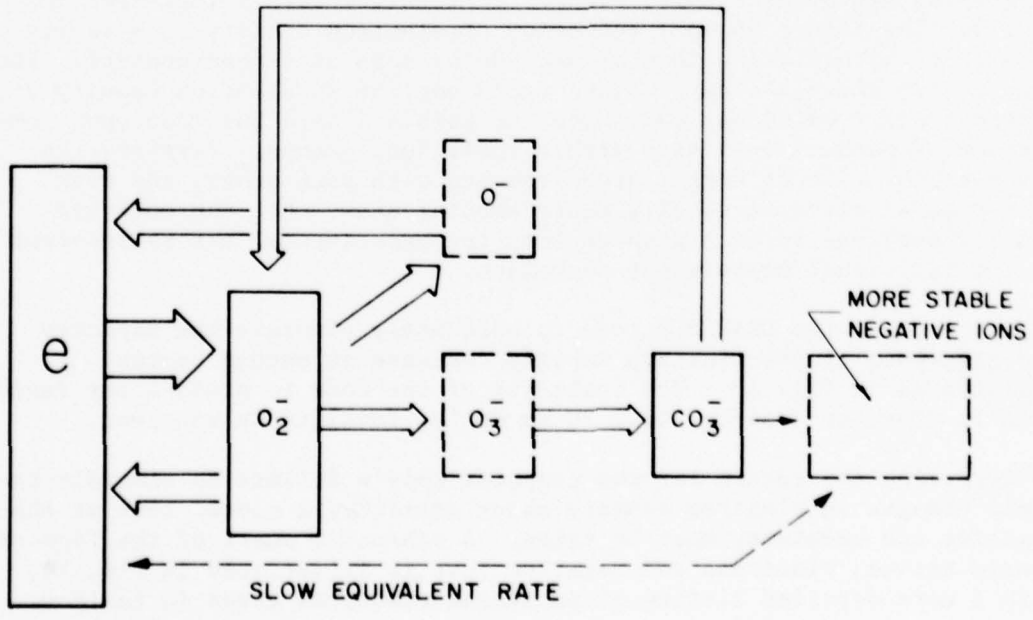

Figure 14. Flow of charge among the negative ions at 2nd contact.

TABLE 6. IMPORTANT ELECTRON ATTACHMENT/DETACHMENT AND CHARGE TRANSFER REACTIONS

Reaction	Critical Minor Species	Rate Constant
$O_3 + e \rightarrow O^- + O_2$	O_3	9.0 (-12)(T/300)$^{1.5}$*
$O_2 + O_2 + e \rightarrow O_2^- + O_2$	-	1.4 (-29)(T/300)$^{-1}$ exp(-600/T)
$O_2 + N_2 + e \rightarrow O_2^- + N_2$	-	1.0 (-31)
$O_2^- + O \rightarrow O^- + O_2$	O	1.5 (-10)
$O^- + O_3 \rightarrow O_3^- + O$	O_3	5.3 (-10)
$O_2^- + O_3 \rightarrow O_3^- + O_2$	O_3	6.3 (-10)
$O_3^- + CO_2 \rightarrow CO_3^- + O_2$	-	5.5 (-10)
$CO_3^- + O \rightarrow O_2^- + CO_2$	O	1.1 (-10)
$O^- + O \rightarrow O_2 + e$	O	2.0 (-10)
$O^- + O_2 (^1\Delta_g) \rightarrow O_3 + e$	$O_2 (^1\Delta_g)$	3.0 (-10)
$O_2^- + O \rightarrow O_3 + e$	O	1.5 (-10)
$O_2^- + O_2 (^1\Delta_g) \rightarrow 2O_2 + e$	$O_2 (^1\Delta_g)$	2.0 (-10)

*Read as 9.0×10^{-12} $(T/300)^{1.5}$; general form A $(T/300)^B$ exp (C/T)

the chain (principally through the intermediate ion O_3^- to CO_3^-) to the more stable negative ion NO_3^-, its hydrates and clusters. No rapid, direct attachment processes of electrons to the more stable negative ions are currently known.

The rate of electron three-body attachment is rapid enough to explain the type of electron density fluctuations shown in fig. 13, but the rate of electron detachment is equally as fast. The species responsible for detaching electrons from O_2^- and O^- are O and $O_2(^1\Delta_g)$. If there were rapid decreases in these latter densities at totality, then perhaps the electrons could stay attached to the O_2^- and O^-, thus accounting for the rapid decrease in the free electron density. Similarly, the crucial minor neutral species responsible for transfer of charge from O_2^- to CO_3^- is O_3. If O_3 were to rapidly increase during totality, then charge could rapidly pass down the negative ion chain and no longer be affected by the rapid detachment processes. However, the time constants for the minor neutral constituents are generally longer than those for ionic species, so that the changes in the O, $O_2(^1\Delta_g)$, and O_3 densities, shown in fig. 15, are relatively smooth and only amount to factors of 2 or 3. The variations needed to explain the observed electron density fluctuations would have to be order of magnitude changes on a time scale of 100 seconds.

Variations in the known reaction rates to simulate a rapid equivalent two-body attachment process involving known species have also been tried [46], but with unsatisfactory results in simulating both the rapidity and magnitude of the electron density decreases.

Therefore, no appeal can be made to the known gas-phase chemistry, which controls the electron attachment and detachment processes, to adequately explain the rapid changes in electron density in the 65 to 85 km region.

SUMMARY AND CONCLUSION

The results of comparing the predictive capabilities of the DAIRCHEM code with the data obtained on the 1966 solar eclipse are summarized as follows:

1. The code provides a good fit to the electron density versus altitude for preeclipse undisturbed conditions.

2. The code prediction of the total positive ion density in the altitude range from about 60 to 85 km at all times is too low by a factor of 2 to 5.

3. The dynamical reduction of the electron density at second contact at altitudes below about 85 km is not predicted by the code.

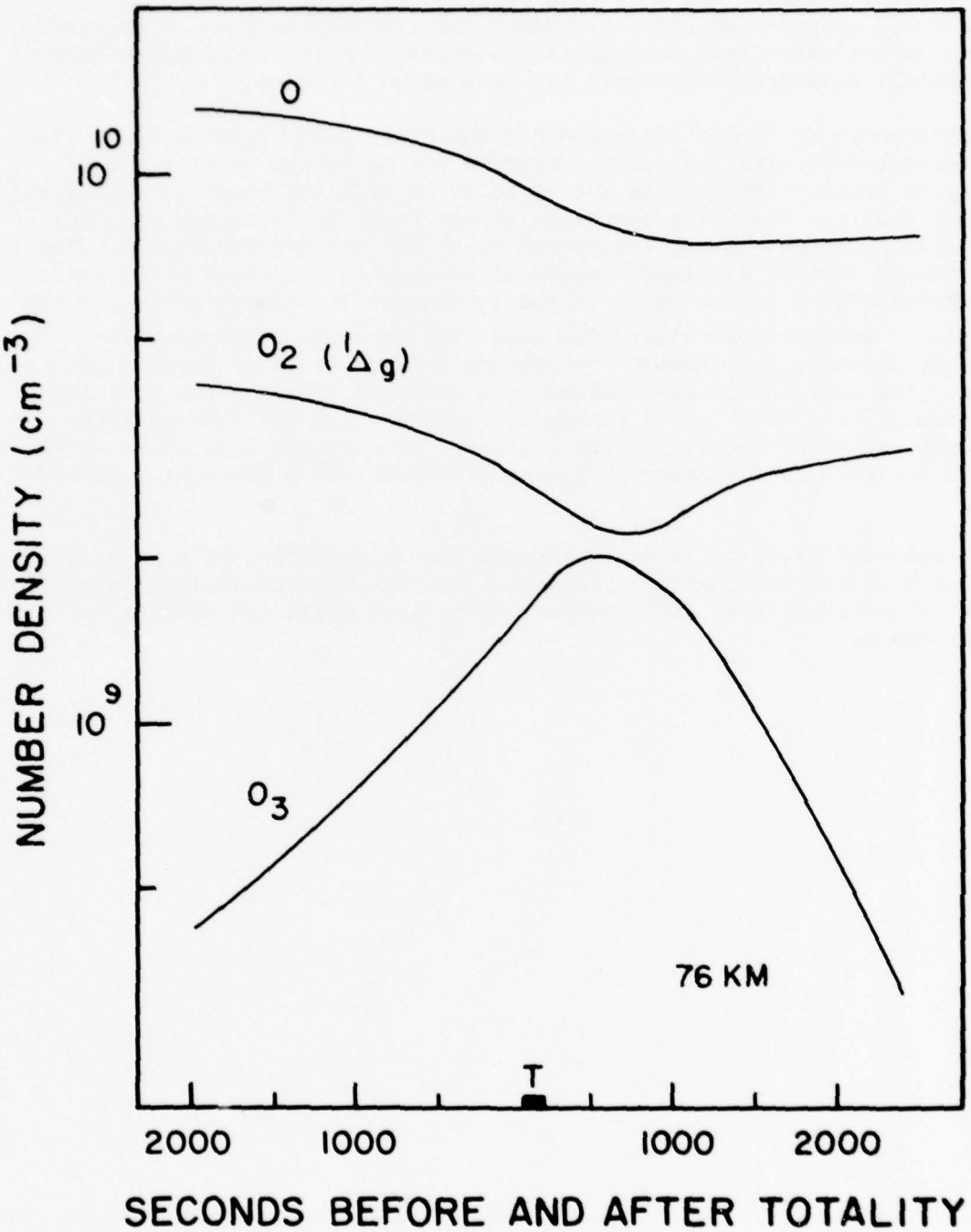

Figure 15. Variation during the eclipse of several of the minor neutral species important in formation of negative ions (O_3) and electron detachment (O and $O_2(^1\Delta_g)$).

4. There are physical limitations on adjusting the reaction rates and processes within the code such that the eclipse data can be fit, especially near second contact. Since the current gas phase chemistry cannot model the actual events, the potential surface chemistry effects of ambient mesospheric aerosols may have to be included.

At this point it is not clear whether the discrepancy between prediction and measurement with respect to positive ion densities or of temporal electron density behavior in the 60 to 90 km altitude range is a failure in the reaction chemistry contained in the code, or is caused by other physical processes in the ionosphere which are not modeled at all. The very rapid fall in electron density at second contact could be explained by attachment to O_2, but only if the subsequent detachment processes are ignored. Another possibility for such rapid changes is by loss to another species, for example, by surface attachment to an aerosol species. The large difference between the observed electron and positive ion density in the 60 to 90 km region, coupled with the fact that the current gas phase chemistry predicts very few negative ions above 70 km, would indicate that negatively charged aerosols are a distinct possibility.

The inclusion of aerosols would require the introduction of a major new set of physical and chemical processes into the conventional mesospheric physics and chemistry, and verification by both field and laboratory experiments.

REFERENCES

1. Sechrist, C. F., Jr., 1972, "Theoretical Models of the D-Region," J. Atmos. Terrest. Phys., 34:1565-1589.

2. Aikin, A. C., 1972, "The Relationship of Theory and Experiment in the D-Region," J. Atmos. Terrest. Phys., 34:1591-1599.

3. Sears, R. D., 1972, "Analysis of the 1966 Solar Eclipse Data," Final Report on contract DASA 01 70 C 0101, Lockheed Palo Alto Research Laboratory Report, LMSC D246526.

4. Mechtly, E. A., K. Seino, and L. G. Smith, 1969, "Lower Ionosphere Electron Densities Measured During the Solar Eclipse of November 12, 1966," Radio Sci., 4:371-375.

5. Lootens, H. T., and W. A. Dean, 1970, "D-Region Electron Density Measurements During the Solar Eclipse of 12 November 1966," US Army Ballistic Research Laboratory Report, BRL R 1464.

6. Sears, R. D., and J. T. Jones, 1965, "Cosmic Noise Absorption Effects of the Eclipse of July 20, 1963," J. Geophys. Res., 70:1207-1214.

7. Sears, R. D., 1965, "Cosmic Noise and VLF Phase Measurements on the Eclipse on May 30, 1965," J. Geophys. Res., 70:5967-5969.

8. Baker, D. C., 1969, "Ionospheric D-Region Parameters from Blunt Probe Measurements During a Solar Eclipse," Pennsylvania State University Report 334B.

9. Ulwick, J. C., 1972, "Eclipse Rocket Measurements of Charged Particle Concentrations," J. Atmos. Terrest. Phys., 34:659-665.

10. Narcisi, R. S., A. D. Bailey, L. E. Wlodyka, and C. R. Philbrick, 1972, "Ion Composition Measurements in the Lower Ionosphere During November 1966 and March 1970 Solar Eclipses," J. Atmos. Terrest. Phys., 34:647-658.

11. Narcisi, R. S., A. D. Bailey, and L. Della Lucca, 1970, "Positive Ion Composition Measurements in the Lower Ionosphere During the 12 November 1966 Solar Eclipse," AFCRL-70-0209.

12. Von Biel, H. A., 1967, "D-Region Partial Reflection Experiment Performed During the 12 November 1966 Solar Eclipse," Cornell Aeronautical Laboratory Report VC 2199-P-1, DASA 1960.

13. Heaps, M. G., 1978, "Parametrization of the Cosmic Ray Ion-Pair Production Rate Above 18 Kilometers," Planetary Space Sci., 26:513-517.

14. Argo, H. V., J. A. Bergey, W. D. Evans, and S. Singer, 1968, "1640A Coronal X-Ray Emission During the 12 November 1966 Eclipse," Solar Physics, 5:551-563.

15. Buchau, J., and G. J. Gassman, "Ionospheric Echo Amplitude Measurements During the 12 November 1966 Eclipse," Paper presented at 1966 Solar Eclipse Symposium, Sao Jose dos Campos, Brazil, February 1968.

16. Ghielmetti, H. S., N. Becerra, A. Godel, H. Heredia, and G. Roederer, 1963, "Enhancement of the X-Ray Intensity at Balloon Altitudes in the South American Anomaly," Phys. Rev. Letters, 12:388-390.

17. Potemra, T. A., and A. J. Zmuda, 1970, "Precipitating Energetic Electrons as an Ionization Source in the Midlatitude Nighttime D-Region," J. Geophys. Res., 75:7161-7167.

18. Eather, R. H., and B. J. O'Brien, 1968, "Photometric Observations in South America and Their Relation to Trapped Radiation," J. Atmos. Terrest. Phys., 30:1585-1590.

19. Walt, M., 1966, "Loss Rates of Trapped Electrons, in 'Radiation Trapped in the Earth's Geomagnetic Field'," ed. B. M. McCormac, D. Reidel Publishing Co., Dordrecht, pp. 337-351.

20. Pfitzer, K. A., and J. R. Winckler, 1968, "Experimental Observation of a Large Addition to the Electron Inner Radiation Belt After Solar Flare Event," J. Geophys. Res., 73:5792-5797.

21. Gassman, G. J., and C. P. Pike, Jr., 1966, "On the Observation of Ionospheric Effects due to Dumping of Trapped Particles, in 'Radiation Trapped in the Earth's Geomagnetic Field'," ed. B. M. McCormac; D. Reidel Publishing Co., Dordrecht, pp. 378-385.

22. O'Brien, B. J., 1966, "Precipitation of Electrons and Protons, in 'Radiation Trapped in the Earth's Geomagnetic Field'," ed. B. M. McCormac, D. Reidel Publishing Co., Dordrecht, pp. 321-336.

23. Rees, M. H., 1963, "Auroral Ionization and Excitation by Incident Energetic Electrons," Planetary Space Sci., 11:1203-1205.

24. Weekes, L. H., 1967, "Lyman Alpha Emission from the Sun Near Solar Minimum," Ap. J., 147:1203-1205.

25. Blamont, J. E., and C. Malique, 1969, "Observation de la Distribution de Brillance a 1216A et 1300A pre du bord solaire," Astron. and Astrophysique, 22:135-146.

26. Accardo, C. A., 1970, "Solar Measurements During the 12 November 1966 Eclipse at Cassino, Brazil," GCA Corporation Report, GCA-TR-70-10-6, DASA 2422.

27. Swider, W., Jr., 1969, "Ionization Rates due to the Attenuation of 1-100A Non-Flare Solar X-Rays in the Terrestrial Atmosphere," Rev. Geophys., 7:573-594.

28. Tousey, R., 1963, "Extreme UV Spectrum of the Sun," Space Sci. Rev., 2:3.

29. Meira, L. G., Jr., 1971, "Rocket Measurements of Upper Atmospheric Nitric Oxide and Their Consequences to the Lower Ionosphere," J. Geophys. Res., 76:202-212.

30. Baker, K. D., A. F. Nagy, R. O. Olsen, E. S. Oran, J. Randhawa, D. F. Strobel, and T. Tohmatsu, 1977, "Measurements of the Nitric Oxide Distribution in the Midlatitude Mesosphere," J. Geophys. Res., 82:3281-3286.

31. Rydbeck, O. E. H., 1946, "Chalmers Solar Eclipse Ionospheric Expedition, 1945," Trans. Chalmers Univ. of Tech., Gothenburg, Sweden, 53, 1946.

32. Pierce, A., and J. H. Waddell, 1961, "Analysis of Limb Darkening Observations," Mem. Roy. Astron Soc., 68:89-112.

33. Meier, R. R., 1969, "Balmer Alpha and Lyman Beta in the Hydrogen Geocorona," J. Geophys. Res., 74:3561-3574.

34. Underwood, J. H., W. S. Muney, and A. C. Aikin, 1968, "Solar X-Ray Emission Characteristics for the Eclipses of May 20th and November 12th, 1966," Solar X-Rays, Sci., 159:383.

35. Accardo, C. A., L. G. Smith, and G. A. Pintal, 1972, "Rocket Observations of Solar X-Rays During the Eclipse of 7 Mar 70," J. Atmos. Terrest. Phys., 34:613-620.

36. Lortie, E. L., M. D. Kregel, and F. E. Niles, 1976, "AIRCHEM: A Computational Technique for Modeling the Chemistry of the Atmosphere," US Army Ballistic Research Laboratories, Report No. 1913.

37. Kregel, M. D., and J. M. Heimerl, 1977, "Comments on the Solution of Coupled Stiff Differential Equations," US Army Ballistic Research Laboratory, Memorandum Report No. 2769.

38. Kregel, M. D., and E. L. Lortie, 1974, "Description and Comparison of the K Method for Performing Numerical Integration of Stiff Ordinary Differential Equations," US Army Ballistic Research Laboratories, Report No. 1733, AD A003855.

39. Kockarts, G., 1976, "Absorption and Photodissociation in the Schumann-Runge Bands of Molecular Oxygen in the Terrestrial Atmosphere," Planetary Space Sci., 24:589-604.

40. Vanderhoff, J. A., 1977, "Photodissociation of $NO^+(NO)$ and $NO^+(H_2O)$," US Army Ballistic Research Laboratory, Report No. 1994.

41. Vanderhoff, J. A., and R. A. Beyer, 1976, "Photodissociation of $O_2^+(H_2O)$," US Army Ballistic Research Laboratories, Memorandum Report No. 2642.

42. Cosby, P. C., J. H. Ling, J. R. Peterson, and J. T. Moseley, 1976, "Photodissociation and Photodetachment of Molecular Negative Ions. III. Ions Formed in $CO_2/O_2/H_2O$ Mixtures," J. Chem. Phys., 65:5267-5274.

43. Niles, F. E., and M. G. Heaps, 1977, "Effects of Photons on Middle Atmospheric Ions," EOS Trans. Am. Geophys. Union, 58:699.

44. Hoock, D. W., and M. G. Heaps, 1978, "DAIRCHEM: A Computer Code to Model Ionization-Deionization Processes in the Middle Atmosphere. A Users Manual," Internal Report, US Army Atmospheric Sciences Laboratory, WSMR, NM.

45. Sears, R. D., 1968, "Research in Connection with HF Propagation, Dayglow Photometry, and VLF Propagation During the 1966 Solar Eclipse," ITT Research Institute Report V6065, DASA 2201.

46. Heaps, M. G., 1978, "The 1979 Solar Eclipse and Validation of D-Region Models," ASL-TR-0002, Atmospheric Sciences Laboratory, White Sands Missile Range, NM.

47. "Solar Geophysical Data," US Department of Commerce Report IER-FB-273, May 1967.

DISTRIBUTION LIST

Dr. Frank D. Eaton
Geophysical Institute
University of Alaska
Fairbanks, AK 99701

Commander
US Army Aviation Center
ATTN: ATZQ-D-MA
Fort Rucker, AL 36362

Chief, Atmospheric Sciences Div
Code ES-81
NASA
Marshall Space Flight Center,
AL 35812

Commander
US Army Missile R&D Command
ATTN: DRDMI-CGA (B. W. Fowler)
Redstone Arsenal, AL 35809

Redstone Scientific Information Center
ATTN: DRDMI-TBD
US Army Missile R&D Command
Redstone Arsenal, AL 35809

Commander
US Army Missile R&D Command
ATTN: DRDMI-TEM (R. Haraway)
Redstone Arsenal, AL 35809

Commander
US Army Missile R&D Command
ATTN: DRDMI-TRA (Dr. Essenwanger)
Redstone Arsenal, AL 35809

Commander
HQ, Fort Huachuca
ATTN: Tech Ref Div
Fort Huachuca, AZ 85613

Commander
US Army Intelligence Center & School
ATTN: ATSI-CD-MD
Fort Huachuca, AZ 85613

Commander
US Army Yuma Proving Ground
ATTN: Technical Library
Bldg 2100
Yuma, AZ 85364

Naval Weapons Center (Code 3173)
ATTN: Dr. A. Shlanta
China Lake, CA 93555

Sylvania Elec Sys Western Div
ATTN: Technical Reports Library
PO Box 205
Mountain View, CA 94040

Geophysics Officer
PMTC Code 3250
Pacific Missile Test Center
Point Mugu, CA 93042

Commander
Naval Ocean Systems Center (Code 4473)
ATTN: Technical Library
San Diego, CA 92152

Meteorologist in Charge
Kwajalein Missile Range
PO Box 67
APO San Francisco, 96555

Director
NOAA/ERL/APCL R31
RB3-Room 567
Boulder, CO 80302

Library-R-51-Tech Reports
NOAA/ERL
320 S. Broadway
Boulder, CO 80302

National Center for Atmos Research
NCAR Library
PO Box 3000
Boulder, CO 80307

B. Girardo
Bureau of Reclamation
E&R Center, Code 1220
Denver Federal Center, Bldg 67
Denver, CO 80225

National Weather Service
National Meteorological Center
W321, WWB, Room 201
ATTN: Mr. Quiroz
Washington, DC 20233

Mil Assistant for Atmos Sciences
Ofc of the Undersecretary of Defense
for Rsch & Engr/E&LS - Room 3D129
The Pentagon
Washington, DC 20301

Defense Communications Agency
Technical Library Center
Code 205
Washington, DC 20305

Director
Defense Nuclear Agency
ATTN: Technical Library
Washington, DC 20305

HQDA (DAEN-RDM/Dr. de Percin)
Washington, DC 20314

Director
Naval Research Laboratory
Code 5530
Washington, DC 20375

Commanding Officer
Naval Research Laboratory
Code 2627
Washington, DC 20375

Dr. J. M. MacCallum
Naval Research Laboratory
Code 1409
Washington, DC 20375

The Library of Congress
ATTN: Exchange & Gift Div
Washington, DC 20540
2

Head, Atmos Rsch Section
Div Atmospheric Science
National Science Foundation
1800 G. Street, NW
Washington, DC 20550

CPT Hugh Albers, Exec Sec
Interdept Committee on Atmos Science
National Science Foundation
Washington, DC 20550

Director, Systems R&D Service
Federal Aviation Administration
ATTN: ARD-54
2100 Second Street, SW
Washington, DC 20590

ADTC/DLODL
Eglin AFB, FL 32542

Naval Training Equipment Center
ATTN: Technical Library
Orlando, FL 32813

Det 11, 2WS/OI
ATTN: Maj Orondorff
Patrick AFB, FL 32925

USAFETAC/CB
Scott AFB, IL 62225

HQ, ESD/TOSI/S-22
Hanscom AFB, MA 01731

Air Force Geophysics Laboratory
ATTN: LCB (A. S. Carten, Jr.)
Hanscom AFB, MA 01731

Air Force Geophysics Laboratory
ATTN: LYD
Hanscom AFB, MA 01731

Meteorology Division
AFGL/LY
Hanscom AFB, MA 01731

US Army Liaison Office
MIT-Lincoln Lab, Library A-082
PO Box 73
Lexington, MA 02173

Director
US Army Ballistic Rsch Lab
ATTN: DRDAR-BLB (Dr. G. E. Keller)
Aberdeen Proving Ground, MD 21005

Commander
US Army Ballistic Rsch Lab
ATTN: DRDAR-BLP
Aberdeen Proving Ground, MD 21005

Director
US Army Armament R&D Command
Chemical Systems Laboratory
ATTN: DRDAR-CLJ-I
Aberdeen Proving Ground, MD 21010

Chief CB Detection & Alarms Div
Chemical Systems Laboratory
ATTN: DRDAR-CLC-CR (H. Tannenbaum)
Aberdeen Proving Ground, MD 21010

Commander
Harry Diamond Laboratories
ATTN: DELHD-CO
2800 Powder Mill Road
Adelphi, MD 20783

Commander
ERADCOM
ATTN: DRDEL-AP
2800 Powder Mill Road
Adelphi, MD 20783
2

Commander
ERADCOM
ATTN: DRDEL-CG/DRDEL-DC/DRDEL-CS
2800 Powder Mill Road
Adelphi, MD 20783

Commander
ERADCOM
ATTN: DRDEL-CT
2800 Powder Mill Road
Adelphi, MD 20783

Commander
ERADCOM
ATTN: DRDEL-EA
2800 Powder Mill Road
Adelphi, MD 20783

Commander
ERADCOM
ATTN: DRDEL-PA/DRDEL-ILS/DRDEL-E
2800 Powder Mill Road
Adelphi, MD 20783

Commander
ERADCOM
ATTN: DRDEL-PAO (S. Kimmel)
2800 Powder Mill Road
Adelphi, MD 20783

Chief
Intelligence Materiel Dev & Support Ofc
ATTN: DELEW-WL-I
Bldg 4554
Fort George G. Meade, MD 20755

Acquisitions Section, IRDB-D823
Library & Info Service Div, NOAA
6009 Executive Blvd
Rockville, MD 20852

Naval Surface Weapons Center
White Oak Library
Silver Spring, MD 20910

The Environmental Research
Institute of MI
ATTN: IRIA Library
PO Box 8618
Ann Arbor, MI 48107

Mr. William A. Main
USDA Forest Service
1407 S. Harrison Road
East Lansing, MI 48823

Dr. A. D. Belmont
Research Division
PO Box 1249
Control Data Corp
Minneapolis, MN 55440

Director
Naval Oceanography & Meteorology
NSTL Station
Bay St Louis, MS 39529

Director
US Army Engr Waterways Experiment Sta
ATTN: Library
PO Box 631
Vicksburg, MS 39180

Environmental Protection Agency
Meteorology Laboratory
Research Triangle Park, NC 27711

US Army Research Office
ATTN: DRXRO-PP
PO Box 12211
Research Triangle Park, NC 27709

Commanding Officer
US Army Armament R&D Command
ATTN: DRDAR-TSS Bldg 59
Dover, NJ 07801

Commander
HQ, US Army Avionics R&D Activity
ATTN: DAVAA-O
Fort Monmouth, NJ 07703

Commander/Director
US Army Combat Surveillance & Target
Acquisition Laboratory
ATTN: DELCS-D
Fort Monmouth, NJ 07703

Commander
US Army Electronics R&D Command
ATTN: DELCS-S
Fort Monmouth, NJ 07703

Commander
US Army Electronics R&D Command
ATTN: DELCS-S (Dr. Swingle)
Fort Monmouth, NJ 07703
3

Director
US Army Electronics Technology &
Devices Laboratory
ATTN: DELET-D
Fort Monmouth, NJ 07703

Commander
US Army Electronic Warfare Laboratory
ATTN: DELEW-D
Fort Monmouth, NJ 07703

Commander
US Army Night Vision &
Electro-Optics Laboratory
ATTN: DELNV-L (Dr. Rudolf Buser)
Fort Monmouth, NJ 07703

Commander
ERADCOM Technical Support Activity
ATTN: DELSD-L
Fort Monmouth, NJ 07703

Project Manager, FIREFINDER
ATTN: DRCPM-FF
Fort Monmouth, NJ 07703

Project Manager, REMBASS
ATTN: DRCPM-RBS
Fort Monmouth, NJ 07703

Commander
US Army Satellite Comm Agency
ATTN: DRCPM-SC-3
Fort Monmouth, NJ 07703

Commander
ERADCOM Scientific Advisor
ATTN: DRDEL-SA
Fort Monmouth, NJ 07703

6585 TG/WE
Holloman AFB, NM 88330

AFWL/WE
Kirtland, AFB, NM 87117

AFWL/Technical Library (SUL)
Kirtland AFB, NM 87117

Commander
US Army Test & Evaluation Command
ATTN: STEWS-AD-L
White Sands Missile Range, NM 88002

Rome Air Development Center
ATTN: Documents Library
TSLD (Bette Smith)
Griffiss AFB, NY 13441

Commander
US Army Tropic Test Center
ATTN: STETC-TD (Info Center)
APO New York 09827

Commandant
US Army Field Artillery School
ATTN: ATSF-CD-R (Mr. Farmer)
Fort Sill, OK 73503

Commandant
US Army Field Artillery School
ATTN: ATSF-CF-R
Fort Sill, OK 73503

Director CFD
US Army Field Artillery School
ATTN: Met Division
Fort Sill, OK 73503

Commandant
US Army Field Artillery School
ATTN: Morris Swett Library
Fort Sill, OK 73503

Commander
US Army Dugway Proving Ground
ATTN: MT-DA-L
Dugway, UT 84022

William Peterson
Research Associates
Utah State University, UNC 48
Logan, UT 84322

Inge Dirmhirn, Professor
Utah State University, UNC 48
Logan, UT 84322

Defense Documentation Center
ATTN: DDC-TCA
Cameron Station, Bldg 5
Alexandria, VA 22314
12

Commanding Officer
US Army Foreign Sci & Tech Center
ATTN: DRXST-IS1
220 7th Street, NE
Charlottesville, VA 22901

Naval Surface Weapons Center
Code G65
Dahlgren, VA 22448

Commander
US Army Night Vision
& Electro-Optics Lab
ATTN: DELNV-D
Fort Belvoir, VA 22060

Commander and Director
US Army Engineer Topographic Lab
ETL-TD-MB
Fort Belvoir, VA 22060

Director
Applied Technology Lab
DAVDL-EU-TSD
ATTN: Technical Library
Fort Eustis, VA 23604

Department of the Air Force
OL-C, 5WW
Fort Monroe, VA 23651

Department of the Air Force
5WW/DN
Langley AFB, VA 23665

Director
Development Center MCDEC
ATTN: Firepower Division
Quantico, VA 22134

US Army Nuclear & Chemical Agency
ATTN: MONA-WE
Springfield, VA 22150

Director
US Army Signals Warfare Laboratory
ATTN: DELSW-OS (Dr. R. Burkhardt)
Vint Hill Farms Station
Warrenton, VA 22186

Commander
US Army Cold Regions Test Center
ATTN: STECR-OP-PM
APO Seattle, 98733

US Army Materiel Systems
Analysis Activity
ATTN: DRXSY-MP
Aberdeen Proving Ground, MD 21005

ATMOSPHERIC SCIENCES RESEARCH PAPERS

1. Lindberg, J.D., "An Improvement to a Method for Measuring the Absorption Coefficient of Atmospheric Dust and other Strongly Absorbing Powders, " ECOM-5565, July 1975.
2. Avara, Elton, P., "Mesoscale Wind Shears Derived from Thermal Winds," ECOM-5566, July 1975.
3. Gomez, Richard B., and Joseph H. Pierluissi, "Incomplete Gamma Function Approximation for King's Strong-Line Transmittance Model," ECOM-5567, July 1975.
4. Blanco, A.J., and B.F. Engebos, "Ballistic Wind Weighting Functions for Tank Projectiles," ECOM-5568, August 1975.
5. Taylor, Fredrick J., Jack Smith, and Thomas H. Pries, "Crosswind Measurements through Pattern Recognition Techniques," ECOM-5569, July 1975.
6. Walters, D.L., "Crosswind Weighting Functions for Direct-Fire Projectiles," ECOM-5570, August 1975.
7. Duncan, Louis D., "An Improved Algorithm for the Iterated Minimal Information Solution for Remote Sounding of Temperature," ECOM-5571, August 1975.
8. Robbiani, Raymond L., "Tactical Field Demonstration of Mobile Weather Radar Set AN/TPS-41 at Fort Rucker, Alabama," ECOM-5572, August 1975.
9. Miers, B., G. Blackman, D. Langer, and N. Lorimier, "Analysis of SMS/GOES Film Data," ECOM-5573, September 1975.
10. Manquero, Carlos, Louis Duncan, and Rufus Bruce, "An Indication from Satellite Measurements of Atmospheric CO2 Variability," ECOM-5574, September 1975.
11. Petracca, Carmine, and James D. Lindberg, "Installation and Operation of an Atmospheric Particulate Collector," ECOM-5575, September 1975.
12. Avara, Elton P., and George Alexander, "Empirical Investigation of Three Iterative Methods for Inverting the Radiative Transfer Equation," ECOM-5576, October 1975.
13. Alexander, George D., "A Digital Data Acquisition Interface for the SMS Direct Readout Ground Station — Concept and Preliminary Design," ECOM-5577, October 1975.
14. Cantor, Israel, "Enhancement of Point Source Thermal Radiation Under Clouds in a Nonattenuating Medium," ECOM-5578, October 1975.
15. Norton, Colburn, and Glenn Hoidale, "The Diurnal Variation of Mixing Height by Month over White Sands Missile Range, N.M," ECOM-5579, November 1975.
16. Avara, Elton P., "On the Spectrum Analysis of Binary Data," ECOM-5580, November 1975.
17. Taylor, Fredrick J., Thomas H. Pries, and Chao-Huan Huang, "Optimal Wind Velocity Estimation," ECOM-5581, December 1975.
18. Avara, Elton P., "Some Effects of Autocorrelated and Cross-Correlated Noise on the Analysis of Variance, " ECOM-5582, December 1975.
19. Gillespie, Patti S., R.L. Armstrong, and Kenneth O. White, "The Spectral Characteristics and Atmospheric CO2 Absorption of the Ho^{+3} YLF Laser at 2.05μm," ECOM-5583, December 1975.
20. Novlan, David J "An Empirical Method of Forecasting Thunderstorms for the White Sands Missile Range," ECOM-5584, February 1976.
21. Avara, Elton P., "Randomization Effects in Hypothesis Testing with Autocorrelated Noise," ECOM-5585, February 1976.
22. Watkins, Wendell R., "Improvements in Long Path Absorption Cell Measurement," ECOM-5586, March 1976.
23. Thomas, Joe, George D. Alexander, and Marvin Dubbin, "SATTEL — An Army Dedicated Meteorological Telemetry System," ECOM-5587, March 1976.
24. Kennedy, Bruce W., and Delbert Bynum, "Army User Test Program for the RDT&E-XM-75 Meteorological Rocket," ECOM-5588, April 1976.

25. Barnett, Kenneth M., "A Description of the Artillery Meteorological Comparisons at White Sands Missle Range, October 1974 - December 1974 ('PASS' - Prototype Artillery [Meteorological] Subsystem)," ECOM-5589, April 1976.
26. Miller, Walter B., "Preliminary Analysis of Fall-of-Shot From Project 'PASS'," ECOM-5590, April 1976.
27. Avara, Elton P., "Error Analysis of Minimum Information and Smith's Direct Methods for Inverting the Radiative Transfer Equation," ECOM-5591, April 1976.
28. Yee, Young P., James D. Horn, and George Alexander, "Synoptic Thermal Wind Calculations from Radiosonde Observations Over the Southwestern United States," ECOM-5592, May 1976.
29. Duncan, Louis D., and Mary Ann Seagraves, "Applications of Empirical Corrections to NOAA-4 VTPR Observations," ECOM-5593, May 1976.
30. Miers, Bruce T., and Steve Weaver, "Applications of Meterological Satellite Data to Weather Sensitive Army Operations,"ECOM-5594, May 1976.
31. Sharenow, Moses, "Redesign and Improvement of Balloon ML-566," ECOM-5595, June, 1976.
32. Hansen, Frank V., "The Depth of the Surface Boundary Layer," ECOM-5596, June 1976.
33. Pinnick, R.G., and E.B. Stenmark, "Response Calculations for a Commercial Light-Scattering Aerosol Counter," ECOM-5597, July 1976.
34. Mason, J., and G.B. Hoidale, "Visibility as an Estimator of Infrared Transmittance," ECOM-5598, July 1976.
35. Bruce, Rufus E., Louis D. Duncan, and Joseph H. Pierluissi, "Experimental Study of the Relationship Between Radiosonde Temperatures and Radiometric-Area Temperatures," ECOM-5599, August 1976.
36. Duncan, Louis D., "Stratospheric Wind Shear Computed from Satellite Thermal Sounder Measurements," ECOM-5800, September 1976.
37. Taylor, F., P. Mohan, P. Joseph and T. Pries, "An All Digital Automated Wind Measurement System," ECOM-5801, September 1976.
38. Bruce, Charles, "Development of Spectrophones for CW and Pulsed Radiation Sources," ECOM-5802, September 1976.
39. Duncan, Louis D., and Mary Ann Seagraves,"Another Method for Estimating Clear Column Radiances," ECOM-5803, October 1976.
40. Blanco, Abel J., and Larry E. Taylor, "Artillery Meteorological Analysis of Project Pass," ECOM-5804, October 1976.
41. Miller, Walter, and Bernard Engebos," A Mathematical Structure for Refinement of Sound Ranging Estimates," ECOM-5805, November, 1976.
42. Gillespie, James B., and James D. Lindberg, "A Method to Obtain Diffuse Reflectance Measurements from 1.0 to 3.0 μm Using a Cary 17I Spectrophotometer," ECOM-5806, November 1976.
43. Rubio, Roberto, and Robert O. Olsen,"A Study of the Effects of Temperature Variations on Radio Wave Absorption,"ECOM-5807, November 1976.
44. Ballard, Harold N., "Temperature Measurements in the Stratosphere from Balloon-Borne Instrument Platforms, 1968-1975," ECOM-5808, December 1976.
45. Monahan, H.H., "An Approach to the Short-Range Prediction of Early Morning Radiation Fog," ECOM-5809, January 1977.
46. Engebos, Bernard Francis, "Introduction to Multiple State Multiple Action Decision Theory and Its Relation to Mixing Structures," ECOM-5810, January 1977.
47. Low, Richard D.H.,"Effects of Cloud Particles on Remote Sensing from Space in the 10-Micrometer Infrared Region," ECOM-5811, January 1977.
48. Bonner, Robert S., and R. Newton, "Application of the AN/GVS-5 Laser Rangefinder to Cloud Base Height Measurements," ECOM-5812, February 1977.
49. Rubio, Roberto, "Lidar Detection of Subvisible Reentry Vehicle Erosive Atmospheric Material," ECOM-5813, March 1977.
50. Low, Richard D.H., and J.D. Horn, "Mesoscale Determination of Cloud-Top Height: Problems and Solutions," ECOM-5814, March 1977.

51. Duncan, Louis D., and Mary Ann Seagraves, "Evaluation of the NOAA-4 VTPR Thermal Winds for Nuclear Fallout Predictions," ECOM-5815, March 1977.
52. Randhawa, Jagir S., M. Izquierdo, Carlos McDonald and Zvi Salpeter, "Stratospheric Ozone Density as Measured by a Chemiluminescent Sensor During the Stratcom VI-A Flight," ECOM-5816, April 1977.
53. Rubio, Roberto, and Mike Izquierdo, "Measurements of Net Atmospheric Irradiance in the 0.7- to 2.8-Micrometer Infrared Region," ECOM-5817, May 1977.
54. Ballard, Harold N., Jose M. Serna, and Frank P. Hudson Consultant for Chemical Kinetics, "Calculation of Selected Atmospheric Composition Parameters for the Mid-Latitude, September Stratosphere," ECOM-5818, May 1977.
55. Mitchell, J.D., R.S. Sagar, and R.O. Olsen, "Positive Ions in the Middle Atmosphere During Sunrise Conditions," ECOM-5819, May 1977.
56. White, Kenneth O., Wendell R. Watkins, Stuart A. Schleusener, and Ronald L. Johnson, "Solid-State Laser Wavelength Identification Using a Reference Absorber," ECOM-5820, June 1977.
57. Watkins, Wendell R., and Richard G. Dixon, "Automation of Long-Path Absorption Cell Measurements," ECOM-5821, June 1977.
58. Taylor, S.E., J.M. Davis, and J.B. Mason, "Analysis of Observed Soil Skin Moisture Effects on Reflectance," ECOM-5822, June 1977.
59. Duncan, Louis D. and Mary Ann Seagraves, "Fallout Predictions Computed from Satellite Derived Winds," ECOM-5823, June 1977.
60. Snider, D.E., D.G. Murcray, F.H. Murcray, and W.J. Williams, "Investigation of High-Altitude Enhanced Infrared Backround Emissions" (U), SECRET, ECOM-5824, *June* 1977.
61. Dubbin, Marvin H. and Dennis Hall, "Synchronous Meteorlogical Satellite Direct Readout Ground System Digital Video Electronics," ECOM-5825, June 1977.
62. Miller, W., and B. Engebos, "A Preliminary Analysis of Two Sound Ranging Algorithms," ECOM-5826, July 1977.
63. Kennedy, Bruce W., and James K. Luers, "Ballistic Sphere Techniques for Measuring Atomspheric Parameters," ECOM-5827, July 1977.
64. Duncan, Louis D., "Zenith Angle Variation of Satellite Thermal Sounder Measurements," ECOM-5828, August 1977.
65. Hansen, Frank V., "The Critical Richardson Number," ECOM-5829, September 1977.
66. Ballard, Harold N., and Frank P. Hudson (Compilers), "Stratospheric Composition Balloon-Borne Experiment," ECOM-5830, October 1977.
67. Barr, William C., and Arnold C. Peterson, "Wind Measuring Accuracy Test of Meteorological Systems," ECOM-5831, November 1977.
68. Ethridge, G.A. and F.V. Hansen, "Atmospheric Diffusion: Similarity Theory and Empirical Derivations for Use in Boundary Layer Diffusion Problems," ECOM-5832, November 1977.
69. Low, Richard D.H., "The Internal Cloud Radiation Field and a Technique for Determining Cloud Blackness," ECOM-5833, December 1977.
70. Watkins, Wendell R., Kenneth O. White, Charles W. Bruce, Donald L. Walters, and James D. Lindberg, "Measurements Required for Prediction of High Energy Laser Transmission," ECOM-5834, December 1977.
71. Rubio, Robert, "Investigation of Abrupt Decreases in Atmospherically Backscattered Laser Energy," ECOM-5835, December 1977.
72. Monahan, H.H. and R.M. Cionco, "An Interpretative Review of Existing Capabilities for Measuring and Forecasting Selected Weather Variables (Emphasizing Remote Means)," ASL-TR-0001, January 1978.
73. Heaps, Melvin G., "The 1979 Solar Eclipse and Validation of D-Region Models," ASL-TR-0002, March 1978.

74. Jennings, S.G., and J.B. Gillespie, "M.I.E. Theory Sensitivity Studies - The Effects of Aerosol Complex Refractive Index and Size Distribution Variations on Extinction and Absorption Coefficients Part II: Analysis of the Computational Results," ASL-TR-0003, March 1978.
75. White, Kenneth O. et al, "Water Vapor Continuum Absorption in the 3.5μm to 4.0μm Region," ASL-TR-0004, March 1978.
76. Olsen, Robert O., and Bruce W. Kennedy, "ABRES Pretest Atmospheric Measurements," ASL-TR-0005, April 1978.
77. Ballard, Harold N., Jose M. Serna, and Frank P. Hudson, "Calculation of Atmospheric Composition in the High Latitude September Stratosphere," ASL-TR-0006, May 1978.
78. Watkins, Wendell R. et al, "Water Vapor Absorption Coefficients at HF Laser Wavelengths," ASL-TR-0007, May 1978.
79. Hansen, Frank V., "The Growth and Prediction of Nocturnal Inversions," ASL-TR-0008, May 1978.
80. Samuel, Christine, Charles Bruce, and Ralph Brewer, "Spectrophone Analysis of Gas Samples Obtained at Field Site," ASL-TR-0009, June 1978.
81. Pinnick, R.G. et al., "Vertical Structure in Atmospheric Fog and Haze and its Effects on IR Extinction," ASL-TR-0010, July 1978.
82. Low, Richard D.H., Louis D. Duncan, and Richard B. Gomez, "The Microphysical Basis of Fog Optical Characterization," ASL-TR-0011, August 1978.
83. Heaps, Melvin G., "The Effect of a Solar Proton Event on the Minor Neutral Constituents of the Summer Polar Mesosphere," ASL-TR-0012, August 1978.
84. Mason, James B., "Light Attenuation in Falling Snow," ASL-TR-0013, August 1978.
85. Blanco, Abel J., "Long-Range Artillery Sound Ranging: "PASS" Meteorological Application," ASL-TR-0014, September 1978.
86. Heaps, M.G., and F.E. Niles, "Modeling the Ion Chemistry of the D-Region: A case Study Based Upon the 1966 Total Solar Eclipse," ASL-TR-0015, September 1978.

☆ U.S. GOVERNMENT PRINTING OFFICE: 1978 777-093/ 20